Profiling float observation of thermohaline staircases in the western Mediterranean Sea and impact on nutrient fluxes

Vincent Taillandier[1], Louis Prieur[1], Fabrizio D'Ortenzio[1], Maurizio Ribera d'Alcalà[2,3], Elvira Pulido-Villena[4]

[1] CNRS, Sorbonne Universités, Laboratoire d'Océanographie de Villefranche, UMR7093, Villefranche-sur-Mer, France
[2] Department of Integrative Marine Ecology, Stazione Zoologica Anton Dohrn, Napoli, Italy
[3] Istituto per lo Studio degli Impatti Antropici e Sostenibilità in Ambiente Marino, CNR, Roma, Italy
[4] Aix-Marseille Université, CNRS, Université de Toulon, IRD, Mediterranean Institute of Oceanography, UMR7294, Marseille, France

Correspondence to: Vincent Taillandier (taillandier@obs-vlfr.fr)

Abstract. In the western Mediterranean Sea, Levantine intermediate waters (LIW), that circulate below the surface productive zone, progressively accumulate nutrients along their pathway from the Tyrrhenian Sea to the Algerian Basin. This study addresses the role played by diffusion in the enrichment of LIW nutrients, a process particularly active inside step-layer structures wide-spread down to deep waters : the thermohaline staircases. In association with the unprecedented contribution of profiling floats to explore their structural changes over long-term scales, the fine characterization of western Mediterranean staircases sampled during the cruise PEACETIME can be carried out from a different perspective. Float observations confirmed that these structures develop over epicentral regions confined inside large scale circulation features and maintained by saltier LIW inflows on the periphery. Thanks to well-adapted sampling rates of some days during a four-years period 2013-2017, float observations reveal the temporal continuity of the layering pattern encountered during the cruise, and, for the Algerian Basin, the evolution of their layer properties by about +0.06°C in temperature and +0.02 in salinity. The analysis of in-situ lateral density ratios is conducted in the view of theoretical models to identify and untangle i) double-diffusive convection as driver of thermohaline changes inside epicentral regions, with ii) isopycnal diffusion as spreader of heat and salt from the surrounding sources. In the Tyrrhenian Sea, the nitrate flux across thermohaline staircases is opposite to the downward salt flux leading to thermohaline changes. It contributes to the accumulation of LIW nitrates up to one fourth of the total contribution by vertical transfer. However, replaced in a larger scope including the action of the biological pump, the enrichment of LIW nutrients is supported more by other sources, coastal or atmospheric, and by the inputs from the Algerian Basin.

1. Introduction

The Mediterranean Sea is an ultra-oligotrophic basin where primary production is generally weak because nutrient fluxes into the sunlit surface layers are very low during most of the year. Apart from dense water formation zones where spring

phytoplankton blooms are observed (D'Ortenzio and Ribera d'Alcalà, 2009), nutrient fluxes and phytoplankton uptake occur mostly at the thermocline (Pasqueron de Fommervault et al., 2015), maintaining a subsurface chlorophyll maximum layer (Lavigne et al., 2013; Barbieux et al., 2019).

Similarly to the global ocean (Williams and Follows, 2003), the Mediterranean nutrient stocks below the thermocline are determined by large scale hydrodynamical transport, following three distinct thermohaline circulation cells (Wüst, 1961). In the western Mediterranean, deep waters (hereinafter DW) result from winter convection in the Provençal Basin and in the Ligurian Sea (Medoc Group, 1970; Prieur et al., 1983). Likewise, the eastern Mediterranean DW are formed in the southern Adriatic Sea and intermittently in the Aegean Sea (Lascaratos et al., 1999; Roether et al., 2007). Mediterranean intermediate waters (hereinafter LIW) originate mostly through shallow convection in different sites of the Levantine Basin (Nittis and Lascaratos, 1999; Malanotte-Rizzoli et al., 2003). The thermohaline circulation cells involving DW are distinct of the eastern or the western Mediterranean basins, whereas the one driven by LIW encompasses the whole Mediterranean. They regionally distribute nutrient stocks, through DW that spread from Liguro-Provençal Basin and from Adriatic-Aegean Seas, or LIW from the eastern Mediterranean (Ribera d'Alcalà et al., 2003; Kress et al., 2003).

Interestingly, the preformed nutrient concentrations in LIW are very low (Pasqueron de Fommervault et al., 2015), they are accumulated along the path, becoming a relevant source of nutrients in the western Mediterranean with nitrate concentration around 5 μmol/kg in the Strait of Sicily. These values are already quite high compared to the intermediate concentrations of the eastern Mediterranean, but correspond to half the concentration measured in the western Algerian Basin (Pujo-Pay et al., 2011). In order to reach such concentrations in the Ionian water inflows, LIW should export the major part of atmospheric and terrestrial inputs from the eastern Mediterranean (Ribera d'Alcalà et al., 2003). Conversely, the mechanisms of LIW enrichment (i.e., accumulation of nutrients in LIW) inside the western Mediterranean are not so clear. External sources (river and coastal runoffs or atmospheric deposition) are larger than in the eastern basin, but the remineralization of organic matter settling from the surface layer becomes a major contributor there (Béthoux et al., 1998). It is worthwhile to note that the LIW enrichment in the Tyrrhenian Sea is comparable to that occurring in the Provençal Basin, as documented by the cruise PEACETIME (Figure 1). This observation has raised our interest on the contribution of alternative processes that could explain such regional modifications in nutrient stocks.

Although the overall distribution of nutrients is driven by large scale circulation, internal processes acting on the vertical scale modify the layout of inorganic matter. This is the case of diapycnal diffusion, which can be particularly efficient when it is enhanced by vertical mixing process due to salt fingering (Hamilton et al., 1989; Fernandez-Castro et al., 2015). Under appropriate conditions reviewed by Schmitt (1994), salt fingering tends to organize the water column into series of mixed layers separated by sharp temperature and salinity gradients, ultimately leading to the formation of thermohaline staircases. Since this natural phenomenon has been elucidated (Stern, 1960; Stern and Turner, 1969), the western Mediterranean Sea has become one of the world's focus for in situ characterization of the resulting step-layer structures. Molcard and Tait (1977) reported the presence of persistent staircases in the central Tyrrhenian Sea, composed of 10 homogeneous layers between 600 m and 1500 m, with constant sea water properties over three years of observation. Later, Zodiatis and Gasparini (1996)

described the areal extent of the structure, covering large distances from the central area, progressively weakening and disappearing near the coasts. Krahmann (1997) reported the first synoptic observations of thermohaline staircases in the Algerian Basin, confirmed by Bryden et al. (2014) from biannual surveys across this region. More recently, Buffett et al. (2017) revealed their remarkable spatial continuity from very high-resolution synoptic observations.

Staircases are thought to be sites of thermohaline changes among well-organized homogeneous layers, when such singular structures are maintained over long terms. Changes can either take the form of intrusions of heat and salt spreading horizontally inside layers (McDougall, 1985; Merryfield, 2000), or slow temporal trends induced by the downward flux of heat and salt between layers (Schmitt, 1994; Radko and Smith, 2012). In order to untangle the two processes, an accurate measurement of thermohaline changes requires temporal continuity of layers, which is the most challenging aspect for observations. Indeed, because thermohaline staircases occur far from the coastal zones and develop at depth, data acquisition is often limited to high resolution but short-term records (e.g. Buffett et al., 2017), or coarse temporal resolution but long-term records (e.g. Falco et al., 2016; Durante et al., 2019). Moreover, most of the existing studies have not considered the role of thermohaline staircases in the nutrient distribution, because pertinent observations of biogeochemical parameters were hard to obtain in the water column at relevant temporal and spatial scales. Profiling floats provide, however, valuable data that can include biogeochemical parameters, allowing to suitably explore the characteristic scales of these features (Biogeochemical-Argo Planning Group, 2016).

In the present study, we focus on the role played by diapycnal diffusion in the distribution of nutrients in the western Mediterranean Sea considering nutrient fluxes between DW, LIW and surface waters, given the regional characteristics of mixing processes. We use the dataset acquired during the cruise PEACETIME (Guieu et al., this special issue), that carried out a large-scale survey of the western Mediterranean Sea in May-June 2017, although data of earlier cruises are also considered. Shipboard data are combined with observations collected by a unique array of Biogeochemical Argo floats deployed in the western Mediterranean Sea (D'Ortenzio et al., 2020). The aim of this study is i) to provide a fine characterization of the staircases recorded by shipboard data, ii) to infer their spatial extension and temporal persistence using profiling float observations, iii) to confirm the occurrence of salt fingering and iv) to assess the contribution of this mixing process in the progressive enrichment and release of LIW nutrients.

2. Data and methods

2.1 CTD profiles

During the cruise PEACETIME in May-June 2017 (Guieu and Desboeufs, 2017; Guieu et al., this special issue), pressure, in situ temperature and conductivity of sea water were measured using SBE911+ CTD from the surface to the bottom. This instrumental package provides continuous acquisitions at 24 scans per second. The depth of each scan is given as pressure (unit: bar). Raw data are processed into quality-controlled profiles of salinity expressed in practical salinity units and potential temperature referenced to surface (0 dbar), at the vertical resolution of 1 dbar (about 1 m). For sake of simplification in the

present study, salinity corresponds to "practical salinity" (no dimension) and temperature corresponds to the derived parameter "potential temperature" (unit: °C). The accuracy of measurement of the CTD unit is about 1 dbar in pressure, 0.001°C in temperature and 0.003 in salinity. The PEACETIME shipboard dataset is complemented with CTD profiles collected during three earlier cruises with same instrumental package, MedSeA (Ziveri and Grelaud, 2015) in May 2013, SOMBA-GE (Mortier et al., 2014; Keraghel et al., 2020) in August 2014, and BioArgoMed (Taillandier et al., 2018) in May 2015.

Another CTD dataset has been collected by profiling floats, autonomous platforms that drift in the interior ocean and evenly surface for positioning and data transmission. The profiling floats considered in this study belonged to the NAOS Biogeochemical (BGC) Argo array (D'Ortenzio et al., 2020). The sampling strategy of this array is better suited for observations of thermohaline staircases than the MedArgo array (Poulain et al., 2007) because the BGC-Argo profiles are deeper, 1000 dbar instead of 700 dbar and remain longer within the deployment basin thanks to a parking depth of 1000 dbar, instead of 350 dbar for MedArgo array. Finally, BGC-Argo floats have higher vertical resolution between 250 and 1000 dbar, 10 dbar instead of 25 dbar for MedArgo array. These floats are equipped with SBE41CP pumped CTDs, sensors of high stability adapted from mooring applications, that provide continuous acquisition at 0.5 Hz with instrumental precision of 0.01 for salinity, 0.002°C for temperature, 2.4 dbar for pressure (Wong et al., 2019). CTD profiles are collected during ascent from the parking depth to the surface, lasting about three hours, with a nominal vertical speed of 0.1 m/s. In the layer between 250 and 1000 dbar, each record is an average of temperature and salinity in 10 dbar bins (about 200 scans), which reduces the noise of raw acquisitions.

The selected BGC-Argo profiles were collected in two regions: (8°E-16°E, 38°N-42°N) in the Tyrrhenian Sea and (2°E-9°E, 36°N-40°N) in the Algerian Basin (Figure 1). The resulting time series of CTD profiles covered four years between May 2013 and May 2017 (date of the cruise PEACETIME) in the first region, it lasted four and half years between May 2013 until December 2017 in the second region (Table 1). The time series have a nominal temporal resolution of seven days that can increase up to one day. In the Tyrrhenian Sea, 323 CTD profiles were collected by two float deployments. The first float 6901491 was deployed in June 2013 during the cruise VENUS2, and recovered while still active two years later in the southwest sector of the basin during the cruise BioArgoMed. The second float 6901769 was deployed immediately (same time and location) following the recovery of float 6901491; it drifted across the Sardinian Channel two years after and was lost in January 2018. In the Algerian basin, 336 profiles were collected by three consecutive float deployments. The first float 6901513 was deployed in May 2013 during the cruise MedSeA, leaving the Algerian basin more than two years later and was recovered in June 2016 in the Provençal Basin during the cruise MOOSE-GE (Testor et al., 2010). The second float 6902732 was refitted from its previous deployment in the Tyrrhenian Sea and deployed at the date and location of the float 6901513 recovery; it entered the Algerian basin offshore Minorca in January 2017 and left the basin one year later. The third float 6901600 was deployed during the cruise SOMBA-GE in August 2014, and was lost in the western part of the basin after more than one year of operation.

Overall, this study encompasses a dataset of about 700 profiles, acquired by BGC-Argo floats at 10-dbar vertical resolution and shipboard CTD package at 1-dbar vertical resolution, with a metrological harmonization at the precision of the BGC-Argo

standards (0.002°C in temperature and 0.01 in salinity). The systematic metrological verification of BGC-Argo CTD sensors, comparing their first profile at deployment with concomitant shipboard CTD profile, confirmed the absence of initial calibration shift for the five floats. This metrological verification has been done also for the recovered floats (6901513, 6901491), which confirmed the absence of temporal drift larger than the nominal uncertainties of CTD measurements.

2.2 Nitrate concentrations

During the cruise PEACETIME, dissolved inorganic nitrate was determined in seawater samples collected by Niskin bottles at discrete depth levels in conjunction with the shipboard CTD profiles. Two distinct sets have been processed (Guieu et al., this special issue): one analyzed within the surface mixed layer at nanomolar concentration levels, and one below analyzed at sub-micromolar concentration levels which in focus for this study. For this latter set, concentrations were measured on board by the standard automated colorimetric method (Aminot and Kerouel, 2007), using a Seal Analytical continuous flow AutoAnalyzer III (AA3). The profiles have with a vertical resolution of 10 m in the surface layer (0-100 dbar), of 50 m in the intermediate layer (100-500 dbar), and of 500 m in the deep layer (below 500 dbar depth until the sea bottom). Note that the sampling of the surface layer has been performed more than once during two long stations in the western Algerian Basin (10 times), and in the central Tyrrhenian Sea (4 times). For the latter station only, the vertical resolution has been increased to 100 m in the upper part of the deep layer (500-1000 dbar).

Another dataset of nitrate concentration has been collected by the BGC-Argo float 6901769 (Table 1). The float was equipped with a Satlantic SUNA-V2 (Submersible Ultraviolet Nitrate Analyzer) sensor, a miniaturized ultraviolet spectrophotometer with which nitrate concentrations can be retrieved from absorbance spectra (Johnson and Coletti, 2002). To do so, a version of the algorithm developed by Sakamoto et al. (2009) has been adapted to the specificity of the Mediterranean Sea (Pasqueron de Fomervault et al., 2015). The SUNA sensor underwent offset and gain corrected by reference measurements at deployment (detailed in Taillandier et al., 2018); its temporal drift was adjusted to a climatological value at 1000 dbar. Overall, a collection of 144 profiles has been acquired in the Tyrrhenian Sea, every five to seven days during a period of two years, with a vertical nominal resolution of 10 m in the upper layer (0-250 dbar) and 25 m in the lower layer (250-1000 dbar).

2.3 Thermohaline staircases

For sake of clarity, the terminology used in the text is illustrated in Figure 2. Thermohaline staircases are observed where large scale temperature and salinity fields decrease with depth in a manner that favors the mixing process of salt fingering (Schmitt, 1994). This natural process has been predicted by theoretical models and reproduced by laboratory experiments and numerical simulations (Schmitt, 1994; Stern and Turner, 1969; Merryfield, 2000; Radko et al., 2014). Salt fingers take the form of tiny cells (some centimeters wide, some tens centimeters tall) across which the rising and sinking fluids mostly exchange heat, as thermal molecular diffusivity is larger than that of salt by two orders of magnitude. In the vertical extension of the cells, sinking (resp. rising) fluids find themselves saltier (resp. fresher), but with same temperature, than waters at the same depth. The resulting buoyancy instability drives convection in the adjoining mixed layers. When salt fingering is active, the whole

transition zone between the warm and salty waters and the cold and fresh waters will be reorganized into mixed layers separated by thin stratified interfaces, until an equilibrium of well-developed staircases is reached (Radko, 2005). The relative stability of this arrangement, whether across a single interface (local) or considering the whole transition zone (bulk), can be expressed in terms of density ratio

$$R_\rho = (\alpha.\partial\theta/\partial z) / (\beta.\partial S/\partial z) \quad (1)$$

which relates the stabilizing vertical temperature (θ) gradient and the destabilizing vertical salinity (S) gradient. α and β are the thermal expansion and haline contraction coefficients of seawater referenced to the same pressure than potential temperature

$$\alpha = -(1/\rho).\partial\rho/\partial\theta \ , \quad \beta = (1/\rho).\partial\rho/\partial S \quad (2)$$

where ρ is the potential density derived from pressure, temperature and salinity using the equation of state of seawater. Based on field observations, low values of density ratio (between 1 and 1.7) are conditional for staircase formation (Schmitt et al., 1987). In the Tyrrhenian Sea and the Algerian Basin, the probability distribution of local density ratios fits the low conditional values (1-1.7) for staircase formation under the LIW core (Onken and Brembilla, 2003).

The detection of thermohaline staircases in the CTD dataset (Section 2.1) is carried out by extracting the depth range of the transition zone for each profile from the salinity maximum (LIW) and the salinity minimum (DW) underneath 250 dbar. The bulk vertical gradients of temperature and salinity are derived from water properties at the top and at the bottom of the transition zone. The resulting bulk density ratio (R_ρ, Equation 1) is checked to be in the range of 1-1.7. Following that, the distribution of pairs (salinity, temperature) that belong to the transition zone is evaluated by a rapid hierarchical classification algorithm in order to detect concentration points representative of mixed layers (Jambu, 1981). A concentration point is identified as a set of successive scans in which temperature does not vary by 0.005°C, salinity does not vary by 0.005. In addition, this set of scans must be composed of at least 3 scans for BGC-Argo profiles, 15 scans for shipboard profiles, limiting the detection to layers thicker than 30 dbar and 15 dbar, respectively. The scans belonging to the concentration points are superimposed onto the full profile and the vertical alternation of interfaces and layers is checked by a visual inspection. After this final step, the profile is reported as an observation of staircases.

Several diagnostics are run on the set of profiles with staircase detection. The fine structure characterization includes layer properties (i.e. seawater temperature and salinity at every validated concentration point), interlayer differences in temperature and salinity, associated interlayer density ratios, layer thickness (i.e. number of concentration points times vertical resolution of profiles), and interface thickness (i.e. the depth interval between two adjacent layers). The occurrence of staircase is estimated among the BGC-Argo dataset by the percent of profiles with at least one concentration point per profile (reported in Table 1). The continuity of layers is displayed among the shipboard and BGC-Argo datasets by the persistence of some layer properties. Layers are conventionally numbered using the fine structure characteristics of the profiles collected during the cruise PEACETIME. Changes of temperature ($\Delta\theta_i$) and salinity (ΔS_i) within every indexed layer (i) are examined among the BGC-Argo dataset in terms of lateral density ratio

$R_L^i = (\alpha.\Delta\theta_i) / (\beta.\Delta S_i)$ (3)

R_L^i are determined by least square fits of layer distributions in a temperature-salinity diagram normalized by β/α.

2.4 Vertical fluxes of nitrate

The vertical transfer of nitrate is parameterized as a diffusive flux, and written as the product of the vertical diffusivity of salts (K) with the vertical gradient in nitrate concentration (C)

$F_{NO3} = K.\partial C/\partial z$ (4)

Fluxes of nitrate are mostly driven by turbulent diffusion, but in presence of thermohaline staircases, the diffusivities of nitrates are enhanced by salt fingering in the same manner than that of salinity (Hamilton et al., 1989). In consequence for the present study, the two mixing processes are considered separately, turbulent diffusion above LIW and salt fingering below LIW, which implies the utilization of alternative formulations for vertical diffusivities.

Above LIW across the nitracline, K is equal to the vertical eddy diffusivity of density, which can be expressed by the buoyancy frequency (N)

$N = (-g/\rho_o.\partial\rho/\partial z)^{1/2}$ (5)

and the turbulent kinetic energy dissipation rate (ε) using the Osborn's (1980) relationship, as

$K_{turb} = \Gamma.\varepsilon / N^2$ (6)

where g is the gravitational constant, Γ is the mixing efficiency, and ρ_o the reference density of seawater. A constant mixing efficiency $\Gamma = 0.2$ is applied under the assumption that the buoyancy Reynolds number

$R_{eb} = \varepsilon / \nu.N^2$ (7)

with kinematic viscosity $\nu = 1.8\ 10^{-6}\ m^2/s$, remains in the range 8.5 – 400 (Bouffard and Boegman, 2013; Ferron et al., 2017). Substituting Eq.(6) in Eq.(4), the vertical flux of nitrate is expressed across isopycnals as the product of ε and the diapycnal gradient of nitrate concentration

$F_{NO3} = - \Gamma.\rho_o/g.\ \varepsilon\ .\ \partial C/\partial\rho$ (8)

This formulation is preferred to the one of Eq. (4) because the temporal consistency in the density-nitrate relationship is stronger than in the depth-nitrate relationship (Omand and Mahadevan, 2015). There were no direct measurements of dissipation rates during the cruise PEACETIME, so we rely on estimates from a Thorpe-scale based parameterization to infer ε values from vertical overturns of density (Dillon, 1982). Following Park et al. (2014), the full resolution CTD records collected in the Tyrrhenian Sea and the Algerian Basin (13 casts) have been reprocessed in order to identify density overturns in the depth interval above LIW, to compute the associated Thorpe scales, and to reconstruct ε profiles. A look-up table composed of ε values averaged over the 13 profiles by 50m vertical intervals is reported in Table 2. The values inside the surface stratified layer (0-100 m) were inconsistent to be considered but the next bin (100-150 m) was kept even if its average value still contains important uncertainties; on the other bins, ε values decrease with depth by one order of magnitude with standard deviations comparable to the average. Combined with a mean N profile, there is an increasing turbulent diffusivity

K_{turb} until the LIW depths where its maximum value is reached. For the surface layer (20-100 m), the look-up table is complemented with ε values of $(6 – 10).10^{-9}$ W/kg, as reported by Cuypers et al. (2012) in the same geographical area. The amplitudes used in the look-up table are in agreement with microstructure observations collected over several cruises from 2012 to 2014 in the same locations (Ferron et al., 2017). These direct measurements documented sharply decreasing ε profiles from values of about 8.10^{-9} W/kg at 100 m down to $0.7.10^{-9}$ W/kg at 300 m. It has to be noted that the assumption of constant mixing efficiency ($\Gamma = 0.2$) is checked with R_{eb} values of about 90 at 100 m and about 80 at 300 m.

Regarding the transition zone below LIW, several formulations of diffusivities across the interfaces of thermohaline staircases have been proposed in the literature, considering different R_ρ-dependent parameterizations inferred by laboratory or numerical experimentations. In the present study, the salt fingering diffusivity of nitrates K_{sf} is parameterized considering the fine characteristics of the step-layer structures observed during the cruise PEACETIME, following three different formulations. Although they have been extensively reviewed and compared between each other, the motivation here is to provide uncertainties on K_{sf} values. First, the formulation of salt fingering buoyancy flux proposed by Schmitt (1981) can be expressed in terms of diffusivity using Eq. (4) as

$$K_{sf} = (0.05 + 0.3 / R_\rho^3). (g. k_T)^{1/3} . (\beta.\delta S)^{4/3} / (\partial S/\partial z) \quad (9)$$

where $k_T = 1.4\ 10^{-7}$ m^2/s is the molecular diffusivity of heat, δS the maximum value of interface salinity differences, $(\partial S/\partial z)$ the mean vertical salinity gradient across the transition layer, and R_ρ the bulk density ratio given by Eq. (1). The second formulation was proposed by Radko and Smith (2012)

$$K_{sf} = k_T.R_\rho.(135.7 / (R_\rho – 1)^{1/2} – 62.75) \quad (10)$$

The third formulation comes from the model of K-profile parameterized diffusivities (Large et al., 1994)

$$K_{sf} = 10^{-4} . (1 – ((R_\rho – 1) / (1.9 – 1))^2)^3 , \quad 1 < R_\rho < 1.9 \quad (11)$$

3. Results

3.1 Observation of staircases in the Tyrrhenian Sea

During the cruise PEACETIME, a station has been performed in the central Tyrrhenian Sea, a well-characterized deep area where intense thermohaline staircases are confined (Molcard and Tait, 1977; Zodiatis and Gasparini, 1996; Falco et al., 2016; Durante et al., 2019). Repeated profiles from the surface to the bottom were collected every day during six days, showing well-ordered thermohaline staircases (Figure 3). At this short observation timescale, there is a strong reproducibility of the vertical structure. LIW properties remain stable at (14.34°C, 38.82), although with a slight uplift of the salinity maximum (470 dbar at cast A, 400 dbar at cast D). DW properties remain equally stable under 2500 dbar at (12.98°C, 38.50). The bulk temperature and salinity gradients are similar for all the casts, respectively 0.00065°C/m and 0.00015/m. The bulk density ratio R_ρ is equal to 1.32, which is lower than 1.7, the upper threshold for the development of thermohaline staircases (Section 2.3). The transition zone is occupied by mixed layers of homogeneous properties (variance close to the instrumental precision) and of various

thicknesses (from few meters to some hundred meters at the metric resolution of the profiles). Interface salinity gradients can be sharp or gradually smoothed by small transient layers that split and merge during the four days of observation. For example, between cast C and cast D (Figure 3), the transient layers disappeared from the interface at 1250 dbar and appeared in the interface at 1700 dbar, meanwhile the layer in between was lifted by about 20 dbar.

Indeed, as reported in Table 3, the layer and interface thicknesses can fluctuate up to 17 dbar during the four days of observation, which are signs of active convection. Instead the temperature-salinity characteristics remain stable. The amplitude of the interface temperature-salinity differences increases with depth until 956 dbar (interface 4/5), then progressively decrease. The three main layers (5, 6, 7) are located between 983 dbar and 1871 dbar depth, with thickness ranging between 184 to 332 dbar. They are associated to large interface temperature-salinity differences, by 0.06-0.19°C and 0.02-0.05.

The spatio-temporal extensions of this observation can be inferred by two BGC-Argo deployments that preceded the cruise PEACETIME. This dataset provides a continuous observation of the vertical structure in the upper 1000 dbar with a resolution of one to seven days from June 2013 until May 2017 (Section 2.1, Table 1). Temperature and salinity scans displayed in the depth range of 300-1000 dbar reveal three stripes at roughly constant properties (Figure 4). The stripes are heavy concentrations of scans that correspond to well-mixed layers, while light concentrations of scans in between the stripes correspond to interfaces. The temperature and salinity values along these stripes are diagnosed by the detection method (detailed in Section 2.3) and analyzed together with the layer properties of the central station (Table 3). The quantification of layer and interface thicknesses can be hazardous on BGC-Argo profiles because of limited vertical resolution, smoothing effects of averaged measurements by 10 dbar slices, and reduction of sensing range (profiling depth equal to 1000 dbar) that may truncate the lowest detected layer. Thus, only the temporal evolution of the layer properties (temperature, salinity) can be considered from the BGC-Argo dataset.

As sketched out in Figure 4, thermohaline staircases were observed almost continuously during the four-years period of BGC-Argo collection. The proportion of staircase detections within this collection reaches 79% (Section 2.3, Table 1). This observation extends over the southwest sector of the Tyrrhenian Sea until the Sardinian Channel (Figure 5, left panel), suggesting a unique structure spreading from the central area up to the southwest border. The obtained vertical structure is in agreement with the ones of shipboard profiles collected at the station PEACETIME and at the float deployment locations two and four years before (Figure 5, right panels). Two layers appear quasi-persistent with steady properties (Figure 5, lower right panels). The first one at (13.65°C, 38.67) corresponds to the layer 3 in the numbering of the station PEACETIME (Table 3), the second one at (13.55°C, 38.65) corresponds to the layer 4. The temperature and salinity gradients at interface 3/4 remain of same amplitude. In complement to this reconstruction of the structure, the layer 2 was detected during two large periods of about one year, the layer 1 during a period of six months, the layer 5 during a short period of three months. As a result, changes on top of the transition zone can whether reduce the number of layers, when LIW are relatively less salty and less warm (second half 2015), or increase the number of layers, while LIW get warmer and saltier (second half 2016). Changes of layer average depth similarly modulate the number of layers, due to vertical translations of the whole structure with the LIW core (Figure 5, upper right panel).

3.2 Observation of staircases in the Algerian Basin

Regarding the Algerian Basin (Figure 6), the CTD dataset covers most of the abyssal plain where thermohaline staircases are able to develop (Krahmann, 1997; Bryden et al., 2014). The cruise PEACETIME provided a zonal transect between 1°E and 8°E with coarse spatial resolution. Three BGC-Argo floats complemented this transect covering the central basin with an average speed of 4 km per day (up to 10 km per day), which is twice larger than that of float motions in the Tyrrhenian Sea. Such a large dispersion in the deep layers (1000 dbar) can be ascribed to a vigorous basin-scale barotropic circulation, characterized by two permanent cyclonic gyres, and delineated by closed f/H contours (Testor et al., 2005). The area of staircase detection (67% of the profiles, Table 1) seems to be shaped by these contours, marking their preferential development inside the so-called Algerian Gyres. More precisely, there is a systematic detection inside the box (37°20'N – 38°N, 4°E – 6°E), whereas staircases were more sporadically observed everywhere else.

During the cruise PEACETIME, four stations have been performed along the 38°N parallel during which nine casts were collected, including six daily casts repeated at a long station (Figure 7). Thermohaline staircases were observed at every station, in the transition zone from the LIW core (300-500 dbar) down to the DW pool (1400 dbar). They exhibit well-ordered steps and layers in the middle of the transect (casts B-H), notably with saltiest observed LIW in cast H, while the profiles at the edges appear jumbled with no readily apparent pattern. In these latter casts A and I, temperature and salinity profiles are inverted within the layers, which reveals lateral intrusions of heat and salt flowing inside the structure along isopycnals. At the long station (casts B-G), the largest steps can be sharp or gradually smoothed by small transient layers that split and merge during the first days of observation. The structure is eroded in the last days (casts F-G), probably due to the growing influence of a mesoscale eddy sampled at the westernmost station (deeper immersion of the LIW core in cast A) progressively moving eastwards at that time.

Even with spatial and short-scale temporal fluctuations, the bulk temperature and salinity gradients remained similar for all the central casts, respectively 0.00060°C/m and 0.00013/m, as well as the bulk density ratio R_ρ equal to 1.38. In a fine description of the vertical structure (Table 4), the transition zone is layered quasi-evenly, with six interfaces of about 0.05°C in temperature and 0.01 in salinity. The largest interface 3/4 separates the two thickest layers (about 70 dbar). Interlayer density ratios decrease from 1.4 to 1.25, with a major variation at the interface 3/4.

The spatio-temporal extensions of this observation can be inferred by the three BGC-Argo deployments that preceded the cruise (Section 2.1). Two separate periods were sampled: from May 2013 until January 2016 then during the whole year 2017 (Table 1). The screening of temperature and salinity scans in the depth range of 300-1000 dbar reveals clear stripes over several periods of some months (Figure 8). In other periods of same duration, the steps are less marked, the concentration of scans between stripes becoming heavier. The continuity of the layers (stripes) is less clear than in the Tyrrhenian Sea, and the sharpness of the steps is more variable (depicted in Figure 8 by different levels of scan concentration between stripes).

The layer properties have been diagnosed by the staircase detection method detailed in Section 2.3. Their evolution is depicted considering the shipboard CTD and BGC-Argo datasets (Figure 9). The profiles collected by the floats, although limited to

1000 dbar, can provide an almost full observation of the vertical structure (the first 5 layers over 7 reported in Table 4). They reveal the reproducibility of the layering pattern over years, in a correct continuity with the one documented in their vicinity by ship surveys. Moreover, gradients at the largest interface 3/4 are in agreement with the values of the stations PEACETIME (Table 4), about 0.07°C in temperature and 0.02 in salinity. Layer properties change when LIW properties suddenly increase, as suggested by the two episodes delimited by red lines in Figures 8 and 9. The two episodes are further analyzed in their geographical context.

During a first episode of three months, the float 6901513 drifted eastwards profiling every 20 km, along a 250-km zonal transect around the 37°30'N parallel (Figure 10, left panel). In contrast with the middle of the transect, the profiles appear jumbled at the eastern and western edges (Figure 10, upper right panel), documenting a disruption of homogeneity within layers and signing lateral intrusions. These local inversions among layers reflect the changes of layer properties reported above (Figure 9), with their slight increase at the beginning of the episode and their decrease at the end. Changes of layer and interface thicknesses can be more clearly documented by a representation of profiles aligned at the depth of the interface 3/4 (Figure 10, lower panel). This representation withdraws the depth fluctuations of layers near the interface 3/4. Staircases appear well developed at the middle of the transect: steps are sharper and layers are thicker than on the two edges, with the apparition of a small transient layer splitting the interface 3/4. This observation suggests well-ordered thermohaline staircases confined inside an epicentral region delineated between 4°15'E and 5°30'E meridians.

During a second episode of four months, the float 6901600 completed a cyclonic gyration, profiling every 10 km along this path of 60 km radius inside the eastern Algerian Gyre (Figure 11, left panel). Lateral intrusions are documented in most of the area crossed by the float (until 22 February 2015, Figure 11 upper right panel), which covers the sector north of the 38°10'N parallel and east of the 5°40'E meridian. In contrast, the layering is sharp and homogeneous for profiles collected in the neighborhood of (37°45'N, 5°20'E). As already described in the first episode, local inversions within layers are associated to changes of layer properties (Figure 9, right panel between red lines). Their intensification increasing with the distance to the location (37°45'N, 5°20'E) documents the development of lateral intrusions on the surrounding.

The two episodes detailed the spatial extension sketched out in Figure 6, with active well-ordered thermohalines staircases confined inside the eastern Algerian Gyre, and their progressive erosion all around. Moreover, these episodes confirmed the connection between layers of fluctuating properties and their continuity over the whole period of observation (suggested in Figures 8 and 9). Positioning layer properties in a temperature-salinity diagram, values are aggregated by layer along separated lines (Figure 12, upper left panel). The float and the cruise records are distributed from the oldest to the newest along these lines, with a succession in time of float 6901513 (blue), SOMBA-GE (purple triangles), float 6901600 (green), PEACETIME (purple dots), and float 6902732 (red). As a result, these lines document a temporal trend at inter-annual scale, as the five connected layers get warmer by about 0.06°C and saltier by about 0.02 during the four years of observation.

The changes of layer properties are examined in terms of lateral density ratio expressed in Eq. (3) and estimated from the slope of layer distributions in the temperature-salinity diagrams (Section 2.3). Their values are reported in Table 5. Considering the whole period, each layer distribution appears shaped along a line crossing isopycnals as a composite of segments nearly parallel

to isopycnals (Figure 12, upper left panel). The gross lateral density ratio associated to this distribution is in the range of 0.65 – 0.78, with an average of 0.72. Considering the episodes separately, their distribution is encapsulated in single segments that have slopes closer to isopycnals (Figure 12, lower panels). Lateral density ratios are in the range of 0.89 – 0.93 for the first episode, 0.82 – 0.98 for the second episode, with an average of 0.91 in both episodes. Given the short timescale of each episode (3-4 months), these ratios are inferred by changes of layer properties attributed to spatial variations, in agreement with the previous geographical description. Considering only the records inside the epicentral region, the distribution extents along lines crossing isopycnals (Figure 12, upper right panel). Lateral density ratios are in the range of 0.74 – 0.83, with an average of 0.80. This ratio is inferred by inter-annual trend in the relative changes between layer temperature and layer salinity. As detailed further in Section 4.3, these estimations of lateral density ratios conjecture water mass conversion within thermohaline staircases that is driven by two distinct processes, one acting at large spatial scales, the other at large temporal scales.

3.3 Estimation of nitrate fluxes in presence of thermohaline staircases

The large-scale distribution of LIW nutrients is examined in the view of the nitrate profiles collected during the cruise PEACETIME in May-June 2017 (Section 2.2). As already pointed out in Introduction (Figure 1), nitrate concentrations progressively increase inside LIW along its pathway from the Ionian Sea to the Algerian Basin. The LIW enrichment is particularly significant in the Tyrrhenian Sea, with an increase by 2 μmol/kg in nitrate concentration between the eastern Tyrrhenian record and the southwestern Sardinian record. This observation is analyzed using five contrasted stations selected along the LIW pathway (Figure 13): in the Ionian Sea upstream the Strait of Sicily, in the southeastern Tyrrhenian Sea downstream the strait, in the central Tyrrhenian Sea, in the continental slope southwest Sardinia, and in the Algerian Basin. Young LIW are found in the Ionian station with strong salinity properties (larger than 38.9) at 200 dbar depth, whereas the lowest LIW properties are found in the Algerian station (salinity 38.6 at 450 dbar). The three other stations have transitional properties, down to 38.7 in salinity southwest Sardinia. Nitrate concentrations follow an inverse progression than salinity: profiles at the five stations are clearly differentiated below 250 dbar, showing inflow of low nutrient waters from the Ionian Sea to the eastern Tyrrhenian (same nitrate values at 450 dbar) and their progressive enrichment until the Algerian Basin.

Focusing now on the central Tyrrhenian Sea and the Algerian Basin where thermohaline staircases act in (Figure 14, left panel), the sunlit surface layers were equally depleted at this period of the year, while the nutrient stocks were similar in the DW with concentrations of about 8.7 μmol/kg in nitrate. Differences appear in the transition zone: vertical gradients of nitrate and salinity are both oriented downwards in the Algerian Basin, whereas they are in opposite direction in the Tyrrhenian Sea. In the first case, nitrate concentrations slightly decrease by 0.7 μmol/kg over a depth range of 500-1500 dbar towards their DW concentrations; while in the second case, the nitrate concentrations increase by 2.3 μmol/kg over a depth range of 500-2000 dbar. A second major difference between the two basins appears on the depth extension of the nitracline. In the Algerian Basin, the base of the nitracline is inside LIW (350-500 dbar), therein nitrate concentrations reach their maximum value maintaining

a downwards gradient with DW stocks. In the Tyrrhenian Sea instead, its extension is limited to 250 dbar: nitrate concentrations reach a local maximum above LIW, then they slightly decrease inside the LIW core (salinity maximum at 400 dbar).

A particular attention is raised on the "S-shape" delineated by the nitrate profile between LIW and the nitracline, marking the isopycnal inflow inside the Tyrrhenian Sea of the nutrient-poor waters from the Ionian Sea. The float 6901769 documented this feature during the two years preceding the cruise. Its dataset is displayed across isopycnals as a narrow range of nitrate profiles around the station PEACETIME (Figure 14, right panel). The S-shape appears as a persistent feature in the southwest sector of the basin, with variable strength depending on the location. It is pronounced in the southeasternmost profiles of the distribution (brown dots), with nitrate concentrations of about 4 μmol/kg along isopycnal 29. Moving west towards the Sardinian Channel, the S-shape is positioned at 5.6 μmol/kg (blue and green dots, Figure 14 right panel). Moving east in the central basin, its minimum increases to 6 μmol/kg (empty dots). Along the eastern Sardinian coast, the S-shape is smoothed to a slight inflexion at 6.5 μmol/kg (red dots). As a result, the Ionian water inflow gradually impacts the nutrient layout above LIW. This will be further discussed with respect to the LIW circulation pathway in Section 4.4.

In the aim to quantify the roles played by thermohaline staircases or Ionian-Algerian inflows on the LIW enrichment, the vertical transfers of nitrates are estimated on three distinct cases: (i) the central Tyrrhenian station of the cruise PEACETIME, with four casts at the same location providing a steady state for density and nitrate concentration, both measured with high accuracy and well-adapted vertical resolution; (ii) the Algerian stations visited by the same cruise, in which spatial and temporal inhomogeneities are introduced, however affecting only the surface layer; (iii) the data collection of the float, with a larger range of situations over seasons and locations (see Figure 5), and less accurate nitrate measurements (Section 2.2). Regarding the two first cases, diapycnal nitrate fluxes are computed using parameterizations detailed in Section 2.4; stages of computation and results are reported in Table 6. For the third case, only diapycnal fluxes above LIW are estimated using the same parameterizations and derived quantities, to access for the representativeness of the fluxes reported in Table 6. A gross nitrate flux has been calculated over 98% of profiles, yielding to estimations of (241 +/- 93) μmol/m^2/d upward through the nitracline, and of (-31 +/- 21) μmol/m^2/d downward from the base of the nitracline into LIW.

The overall distribution of the nitrate transfers along a zonal transect crossing the southwestern Mediterranean is displayed in Figure 15. It appears that the largest fluxes correspond to the nutrient supply in the surface productive waters. Regarding LIW stocks, there is a loss of nitrate in the Algerian Basin, mostly towards the surface layer, whereas in the Tyrrhenian Sea, there is an enrichment. The contribution from the DW reservoir through thermohaline staircases represents one fourth of that supply; considering that LIW receives also nitrates from above during Tyrrhenian transit, LIW is a net exporter of nutrients from the basin. The implications will be further discussed in comparison with other processes in Section 4.4.

4. Discussion

4.1 Different vertical structures

The two staircase regions crossed by the cruise PEACETIME have displayed different layering aspects. In the Tyrrhenian Sea, thermohaline staircases are the predominant feature of CTD profiles (Figure 3); they spread over most of the water column from 600 to 2275 dbar; they are made up of ten mixed layers that can reach atypical thicknesses of 330 m. Only the upper part of the structure has been observed by the BGC-Argo floats because their profiling depth was limited to 1000 dbar. On the other hand, the thermohaline staircases of the Algerian Basin are well documented by the BGC-Argo collection; they extend between 600 and 1200 dbar depth (Figure 7), with seven mixed layers of thickness 30-75 m. How to explain these structural differences between two basins occupied by the same water masses? One reason is the inflow of newly formed DW in the Algerian Basin: denser than the old ones, they lay on the seafloor up to 2300 dbar (Figure 7) uplifting the "older" DW (Zunino et al., 2012; Send and Testor, 2017). Consequently, the DW pool presents a temperature-salinity minimum at 1400 dbar that intrinsically limits the vertical extension of the structure. In the Tyrrhenian Sea, the transition zone is not bounded so that staircases can extend over larger depths. On the other hand, Tyrrhenian LIW are warmer and saltier than Algerian LIW, they favor low density ratios which drive preferential development of large layers (further detailed below in this Section 4.1).

The thermohaline staircases observed during the cruise PEACETIME have similar characteristics than that previously reported in the same basins. Regarding the Tyrrhenian Sea, the vertical structure is very close to those observed in 2007-2010, reported by Falco et al. (2016), and more interestingly, to the one observed 44 years ago, in May 1973, reported by Molcard and Trait (1977). Meanwhile, Zodiatis and Gasparini (1996) observed a lower number of layers inside the same vertical extension (only 6 in 1991, even 5 in 1992), together with larger individual thicknesses (up to 543 m). Notably, the DW properties were modified during this period as an effect of the eastern Mediterranean transient (Gasparini et al., 2005): the observed injection of heat and salt in the deep Tyrrhenian Sea would have favored the lowest layers to merge. Moreover, Durante et al. (2019) documented an upward lift of the vertical structure by several hundred meters after 2010, and the presence of smaller steps below the deepest thick step, which is likely due to the ingression of a new denser water mass from the large production of anomalous DW in the Liguro-Provençal basin during the winters 2005 and 2006. Regarding the Algerian Basin, the present vertical structure is close to the ones observed in 1994, reported by Krahmann (1997). At that time, the vertical structure extended between 500 and 1300 dbar, with seven layers of thickness ranging between 28 m and 67 m in average over two field surveys in winter and autumn. Considering another report by Bryden et al. (2014) from biannual surveys between 2006 and 2010, the transition zone extended in depth, however limited by a temperature-salinity minimum at 1600 dbar, with eight layers averaging 93 dbar in thickness and a bulk density ratio of 1.28. In comparison with the present observation, an uplift of the "old" DW by 200 m and an increase of the density ratio to 1.38 could explain such structural differences.

As sketched out above, layers tend to be thicker when bulk density ratios decrease. The theoretical model of Radko (2005) describes the macroscopic formation of thermohaline staircases by salt fingering as a series of merging events that make thin and unsteady layers grow into an equilibrated vertical structure. At this ultimate state, layer thicknesses reach a critical value

determined by the bulk density ratio (see the Figure 3 of Radko, 2005). The model predicts critical heights to drop down with increasing bulk density ratios, about 200 m for bulk density ratios of the Tyrrhenian Sea (1.32) and about 80 m for those of the Algerian Basin (1.38). According to the present observations (Tables 3 and 4), the critical heights of layers in the middle of the structure are in good agreement with the model predictions. Moreover, following Radko et al. (2014), there is a tendency for unsteady layers to merge if the height of the adjoining layers is lower than their critical value; the preferential merging scenario, denominated "B-merger", should be realized in a manner that temperature-salinity differences between thick layers is maintained. This mechanism of adjustment has been recorded in the present observations. The daily profiles at long stations in the Tyrrhenian Sea (casts A-D, Figure 3) and in the Algerian Basin (casts B-G, Figure 7) documented the occurrence of small transient layers at the interface between layers that have likely reached their critical height, without any change of layer properties. In addition, the two sequences of BGC-Argo profiles in the Algerian Basin (Figures 10 and 11) also documented the occurrence of a small transient layer that whether splits the main interface 3/4 when the adjacent layers are large or merges when the adjacent layers shorten, while the interlayer temperature-salinity gradients remain equal.

4.2 Areal extents delineated by large scale circulation features

In this section, the spatial extension of the staircase regions is first compared to previous observations, then discussed in the view of underlying circulation features. In the Tyrrhenian Sea, the present analysis suggests a unique structure spreading from the central area until the southwest border (Figure 5). According to Zodiatis and Gasparini (1996) who studied a set of cross-shore transects all around the basin, thermohaline staircases cover large distances from the central part, becoming progressively weaker and finally disappearing near the borders. The authors reported an extension in the southwestern sector of the basin, documented along two cross-shore transects southeast Sardinia, which is in agreement with the present case (Figure 5, left panel). Sparnocchia et al. (1999) confirmed such extension in the northwest of Sicily. More recently, high-resolution synoptic observations of staircases by seismic data have been reported along three zonal transects north of the 40°N parallel (Buffett et al., 2017). The staircases are depicted as continuous stripes, well-ordered in the central part of the basin, weakening close to the continental slope, with a remarkable spatial continuity. This beam of independent observations confirms the hypothesis of a unique structure extending over large parts of the Tyrrhenian Sea, with an epicenter located at its deep central area, as proposed by Molcard and Tait (1977).

Such epicentral configuration, with active salt fingering (see Section 4.3) and well-developed staircases that progressively erode while moving away, can also be applied to the case of the Algerian Basin. The basin-scale survey by BGC-Argo floats pointed out a region of systematic staircase detection around (37°45'N, 5°20'E) extending west until the 4°E meridian and south until the 37°20'N parallel. In addition, the zonal transect of the cruise PEACETIME, although of coarse resolution, showed a well-developed vertical structure in this region (cast 8, Figure 7). Thermohaline staircases have been previously observed along the same zonal transect (Bryden et al., 2014). Thanks to biannual surveys at higher spatial resolution, the authors reported the different layering aspects: well-ordered vertical structures around 4°E progressively eroded westwards, and jumbled profiles at the eastern stations. More recently, glider surveys along the 3°E and 4°E meridians provided high

resolution synoptic observations of thermohaline staircases with a remarkable spatial continuity between the different layering aspects (Cotroneo et al., 2019). These reports are in agreement with the regionalization by staircase regimes proposed by Krahmann (1997): a region of inverted layers close to Sardinia where LIW enter the basin and flow northwards along its coast, a band around the first of well-ordered layering, and a region further west with "diffusively reduced" layers.

If DW play a role on the vertical extension (Section 4.1), areal extents of thermohaline staircases appear to be controlled by LIW circulation features. In other terms, locally high LIW properties, originating whether from the southeast or from southwest Sardinian sectors, would drive the same epicentral configuration for the two staircase regions. Warmer and saltier LIW are brought throughout the Strait of Sicily by the eastern Mediterranean outflow that directly sinks inside the Tyrrhenian Sea. Following Sparnocchia et al. (1999), the flow is made up of LIW at 200-800 m depth and transitional DW detected down to 1850 m depth. The authors argued that the mixing by salt fingering process acts when the bottom slope does not influence the vein any more. On the other side of the Sardinian Channel, the LIW vein flowing inside the Algerian Basin is warmer and saltier than the central Algerian waters. The vein circulates northward along the continental slope, delineated by a density front along which interleaving layers are triggered (Krahmann, 1997).

The influence of young LIW intrusions inside the adjoining basins can extend over large distances. In the case of the Tyrrhenian Sea, the deep circulation is weak enough that young LIW, progressively entrained cyclonically along the continental slope, affect the central basin through lateral intrusions (Zodiatis and Gasparini, 1996). In the case of the Algerian Basin, the eastern Algerian Gyre, a component of the basin-scale barotropic cyclonic circulation (Testor et al., 2005), plays a stabilizing role for interleaving layers to take the form of thermohaline staircases, and extend westwards until the epicentral region. Interesting to note, LIW are observed warmer and saltier in the western part of the gyre (between 4°E and 6°E) even if it is the part of the gyre farthest from the inflow of young LIW (Mallil et al., 2016). The anomaly is also sketched in the transect PEACETIME: the cast 8 located in the western part of the gyre presents saltier LIW than that of cast 9 located in its eastern part (Figure 7). This patch matches with the epicentral region where staircases become active and well-developed (Figure 6). The origin of this patch can be inferred from specific mesoscale structures: the Sardinian eddies. They are anticyclones with a deep LIW core (600 m depth) that detach from the continental slope and evolve at the periphery of the eastern Algerian gyre (Testor and Gascard, 2005). As a result, young LIW transported by Sardinian eddies likely end up confined in the western part of the gyre with slightly modified properties. In addition, the float 6901513 has been trapped three times inside Sardinian eddies. This is signed by the high anomalies of LIW properties (Figure 9), and deeper LIW core as profiles truncated by the 1000 m profiling depth are observed with narrower temperature-salinity ranges (see Figure 8). Two events of July 2013 and July 2014 were located in the northern part of the western Algerian Gyre (39°N, 5-6°E), one event of March-April 2015 was located along the eastern border of the basin.

4.3 Temporal continuity and water mass conversion

The temporal continuity of thermohaline staircases is the most challenging aspect to assess from observations. In the present study, the large timeseries collected by the BGC-Argo floats with a resolution of some days revealed the continuity of the

layering pattern over months and years (Figures 4, 8). As a result, adjustments of the vertical structure, or even their decay, have been documented at short timescales (some days) in response to changes of LIW characteristics (changes of immersion or properties, Figures 5, 9). In the case of the Algerian Basin, these changes have been analyzed under the caveat of rapid float motions as resulting spatial variations may insert distortions (Figure 10, 11). Thanks to the BGC-Argo collection, thermohaline staircases are found long-lived, whether in the Tyrrhenian Sea in agreement with the early estimate of Molcard and Tait (1977), or in the Algerian Basin.

Quasi-permanent staircases are thought to be sites of thermohaline changes among continuous mixed layers, characterized according to two specific regimes and identified by range values of lateral density ratios (R_L, Equation 3). In a first regime, thermohaline changes can take the form of intrusions of heat and salt spreading horizontally inside layers. This spatial regime is triggered and sustained by isopycnal stirring from a steady interleaving state (McDougall, 1985; Merryfield, 2000), which would yield to lateral density ratios close to 1 (Schmitt, 1994). Alternatively, thermohaline changes can take the form of slow temporal trends induced by the downward flux of heat and salt. In this temporal regime, the lateral density ratio is identifiable with the convergence flux ratio that relates heat and salt fluxes across salt fingers (Schmitt, 1994). Observations often provide a mixture of the two regimes (Schmitt et al., 1987), nevertheless the relative changes in layer properties can be documented whether spatially with synoptic surveys, or temporally with long term records at fix locations. Lateral density ratios derived from observations can be compared to theoretical models in order to identify whether isopycnal stirring or salt fingering is active. As sketched out in Section 3.2, the present estimations of lateral density ratios can be characteristic of one of the two regimes specifically, depending on the spatial or temporal limitations of the considered distributions.

To the best of our knowledge, in situ measurements of lateral density ratios at inter-annual scales, with a resolution ensuring the continuity of the layers among the vertical structure, are made for the first time available for the western Mediterranean achieved by the present BGC-Argo collection. Lateral density ratios have been evaluated in the Tyrrhenian Sea (Zodiatis and Gasparini, 1996) as well as in the Algerian Basin (Krahmann, 1997) considering synoptic field surveys. Their results are in agreement with the theoretical prediction of the spatial regime with values close to 1. An attempt of evaluation of long-term trends using historical data has been proposed by Zodiatis and Gasparini (1996), but the fluctuations encountered in the vertical structure (detailed in Section 4.1) did not lead to any reliable estimate of lateral density ratio within single and continuous layers. Falco et al. (2016) provided interannual trends of vertical averaged properties, which could neither give access to any estimate of lateral density ratios.

The layer temperature and salinity changes have been analyzed in both spatial and temporal scales using the BGC-Argo collection. Regarding the Tyrrhenian Sea, the two floats drifted slowly in the southwest sector, moving progressively away from the epicenter. An estimate of long-term trends would be affected by such a slow spatial motion, with the challenge to be untangled from spatial variations. Moreover, only the upper vertical structure has been sampled by the floats (until 1000 dbar), more likely affected by adjustments and inversions among layers because the eastern Mediterranean flow is preferentially injected in that depth range (Sparnocchia et al., 1999). As a result, the consequent fluctuations reach the order of instrumental

precision (0.01 in salinity), so the estimation of any lateral density ratio has been discarded and not reported for the Tyrrhenian Sea in the present study.

On the other hand, the more dynamical situation of the Algerian Basin provided extensive and synoptic surveys of the area, with several pathways across the eastern Algerian gyre. In particular, the duration of the BGC-Argo timeseries allowed to assess variations of layer properties larger than the instrumental precision limit, with about 0.02 in salinity during the four years of acquisition. The collection gives access to the main layers (3 and 4) and the largest steps (interface temperature-salinity differences larger than instrumental precision) of the vertical structure, which separates the layer properties and reduces the noise in the slope estimates. The resulting distributions lay out in a temperature-salinity diagram as a superimposition of episodes marked by distinct segments with an overall trend, where the two regimes of water mass conversion appear untangled (Figure 12). Lateral density ratios have been found to 0.91 from distributions limited to short episodes. This is in agreement with theoretical results of thermohaline changes driven by isopycnal intrusions (McDougall, 1985; Merryfield, 2000). When the distribution is limited to the western sector of the eastern Algerian Gyre (epicentral region), the lateral density ratio drops down to values in the range of 0.74-0.83 depending on layers. When the whole dataset is considered, the gross lateral density ratio reaches an average value of 0.72. These estimations can be compared to the theoretical flux ratios, equal to 1 for isopycnal stirring process, that drop down to 0.5-0.7 when salt fingering is active (Schmitt et al., 1987). Flux ratio predicted by the model of Radko and Smith (2012) is 0.60 using bulk density ratio of the Algerian Basin (1.38). This result consolidates the diagnostic based on layering patterns of active salt fingering in the western sector of the eastern Algerian Gyre.

4.4 LIW nitrate enrichment in the Tyrrhenian Sea

The nutrient pool below the surface productive waters is interconnected over the whole Mediterranean by the thermohaline circulation. LIW are thought to act as conveyor belt that progressively accumulate nutrients from the eastern to the western basins of the Mediterranean Sea. During the cruise PEACETIME, LIW enrichment has been particularly observed across the Tyrrhenian Sea: nutrient concentrations increased by 2 µmol/kg in nitrate within a layer of 100 m thickness (Figures 1 and 13). Vertical transfers of nutrients by diffusion would likely contribute to this enrichment, and this for two reasons. First, thanks to the presence of thermohaline staircases, the salt fingering diffusivity has been evaluated about three times larger than the turbulent diffusivity reported by Ferron et al. (2017) in the depth range of 1000-2000 m, which is in agreement with the theoretical prediction of Hamilton et al. (1989). Second, the eastern Mediterranean LIW flowing inside the Tyrrhenian Sea with low nutrient concentrations are able to reverse and accentuate the vertical gradient with DW stocks, which originate mostly from the Algero-Provençal Basin (Figure 13). As a result from the analysis of the PEACETIME dataset, the nitrate flux between DW and LIW is opposite to the flux of salt; it contributes to one fourth of the nitrate supply inside LIW, the three other fourths are provided by nutrients coming from above LIW (Figure 15). However, the cumulated vertical fluxes of nutrients, reaching values of 10.9 – 39.3 µmol/m^2/d in nitrate, are not sufficient to explain the observed increase of LIW nutrients in the Tyrrhenian Sea: the associated duration for vertical nitrate fluxes to balance their 2 µmol/kg increase is in the

range of 14 – 60 years. This is not consistent with the magnitudes of LIW residence times inside the Tyrrhenian Sea, about some years with respect to dispersion time scales at 350 m from MedArgo floats (Poulain et al., 2007).

In addition to vertical diffusion, horizontal advection by large-scale circulation could also contribute to the observed modifications of nutrient content in the Tyrrhenian Sea. The Ionian vein flowing through the Sicily Strait has a bounded extension: the interface at 200 dbar depth delineates the upper limit with the layer above occupied by the modified Atlantic water outflow; the depth of the sill (480 m) delineates its lower limit. In consequence for the Tyrrhenian waters, the surface layer (above 200 dbar) is not influenced by the Ionian inflow; the deep layer (below 500 dbar) is quickly and locally affected by the cascading of the dense Ionian waters that are modified by turbulent mixing with DW until they reach their level of equilibrium (between 500 and 1400 dbar, Sparnocchia et al., 1999). As evidenced in Figures 13 and 14, only the layer between 200 and 500 dbar gradually changes its large-scale properties and increases its nutrient concentrations over the whole Tyrrhenian Sea. Focusing on this depth range, there is an overall agreement between the signature of Ionian LIW (the S-shape on nitrate profiles, Figure 14) and the pathway of LIW circulation (Krivosheya and Ovchinnikov, 1973; Astraldi and Gasparini, 1994). The strongest perturbations of nitrate layout are located at the southwestern sector (brown, red and blue dots, Figure 14) corresponding to the branch of circulation between the Sicily Strait and the Sardinian Channel. This pattern is smoothed along the eastern Sardinian coast (red dot, Figure 14) in correspondence with the branch of LIW outflow. Note that the regional circulation scheme of Krivosheya and Ovchinnikov (1973) also reports the inflow of Algerian waters in the surface layer along the southern border of the basin: the presence of this nutrient-rich water mass above LIW accentuates the contrast with nutrient-poor Ionian waters and the perturbation of nitrate layout reported in the southwestern sector of the Tyrrhenian Sea (Figure 14, right panel). We should add another physical process that might contribute to LIW enrichment: the contribution of terrestrial inputs by isopycnal diffusion at the 400-500 dbar depth horizon of the LIW. These inputs would be transferred to the intermediate layer by the biological pump along the Tyrrhenian shelves, then advected by lateral intrusions that develop along the continental slope and feed the thermohaline staircase in the central part of the basin (Zodiatis and Gasparini, 1996; Sparnocchia et al., 1999).

The contribution of physical processes should be replaced in a larger scope, including the action of the biological pump that resupplies in nutrients the waters below the surface productive layer through remineralization of organic matter and export, including also the contribution of external sources such as atmospheric deposition. The upward flux of nitrates to the surface layer estimated in the present study (420 – 700 μmol/m^2/d, Figure 15) has the same order of magnitude than direct measurements in the northwestern Mediterranean Sea during late spring (Mouriño-Carballido et al., 2016); it corresponds to 11 – 20 gC/m^2/y of new production in carbon. Alternatively, a very crude calculation considering the increase of LIW nitrate concentration by 2 μmol/kg in its passage through the Southern Tyrrhenian Sea would lead to new production of ~30 gC/m^2/y, assuming a LIW transport of 1 Sv and a Southern Tyrrhenian surface of 150000 km^2. These independent estimations are close to new production values of 10 gC/m^2/y calculated from the phosphorus budget in the Tyrrhenian Sea (Béthoux, 1989). Annual carbon fixation rates, equivalent to total production, were estimated to 87 gC/m^2/y from ocean color imagery in the Tyrrhenian

Sea (Morel and André, 1991). This means that to support the observed total production the LIW nitrogen should turnover 5.4 times in the productive layer with an hypothetical f-ratio of 0.18, in agreement with f-ratio values of other oligotrophic areas. All this depicts a more complex scenario. Contrary to what could have been supposed looking at the strong nutrient gradient between LIW and DW at the southeast entrance of the basin, the nutrient stock accumulated by LIW along the path in the eastern Mediterranean Sea, is not the main fertilizer of the Tyrrhenian Sea. Instead the basin primary production is supported more by other sources, coastal or atmospheric, within the basin and, possibly, by the inputs from the Algerian Basin. The latter inputs arrive very likely in organic forms in the layer above 100 m (Santolleri et al., 2018), since existing data do not show significant inorganic nutrients concentrations in the surface along the Sardinian Channel (e.g., Astraldi et al, 2002), and also in inorganic forms that are entrained below the surface in the Algerian Basin. These nutrients are utilized within the basin, biologically pumped down into the LIW and exported to the Algero-Provençal Basin, more than compensating the surface and deep inputs from the latter. Overall the Tyrrhenian Sea acts as a remineralization basin and as a source of nutrients for the Algero-Provençal Basin more than a sink for the eastern originating nutrients.

5. Conclusion

Having examined CTD profiles of BGC-Argo datasets and field surveys, we report long-term observations of thermohaline staircases in two sites of the western Mediterranean: the Tyrrhenian Sea and the Algerian Basin. In association with the unprecedented contribution of profiling floats to explore the structural changes of thermohaline staircases, at high resolution and during several years, their fine characterization carried out by the cruise PEACETIME can be seen from a different perspective.

In the two sites, the staircases develop in the transition zone between LIW and DW, over areal extents organized around epicentral regions. These epicentral regions are located inside large scale circulation features, that stabilize the influence of interleaving layers triggered by saltier LIW inflows. As observed in the Algerian Basin, epicentral regions are sites of active mixing, with changes of seawater properties by about +0.06°C in temperature and +0.02 in salinity during the four years of observation. The dataset collected by profiling floats gave access to the measurement of in-situ lateral density ratios over inter-annual scales, with a resolution ensuring the continuity of the layers among the vertical structure. These lateral density ratios have been analysed in the view of theoretical predictions to identify and untangle i) salt fingering as driver for water mass conversion, with ii) isopycnal diffusion as spreader of heat and salt from the surrounding sources.

Thermohaline staircases represent remarkable locations of enhanced diapycnal diffusivity for inorganic nutrients. In addition to large-scale advection and isopycnal stirring, they actively participate to the LIW nitrate enrichment across the Tyrrhenian Sea, together with the remineralization of particulate biogenous material produced in surface or dissolved organic matter coming from Algerian Basin and Tyrrhenian coastal areas. The respective role of these sources and process contributions for LIW enrichment has been first guessed in the present study and would require deeper investigations, in particular addressing nitrate accumulation in conjunction with apparent oxygen utilization along the LIW pathway and their agreement with Redfield

utilization ratio. A more detailed picture of the long-term evolution of Tyrrhenian staircases and interplay with nutrients will undoubtedly emerge with in course deployments of BGC-Argo floats embarking nitrate and oxygen sensors.

Author contribution

VT, LP and FDO contribute to the experimental setup, to the data analysis and to the writing of the manuscript. MRA and EPV contribute to the analysis of nutrient data and to the review of the manuscript.

Acknowledgments

This study is a contribution to the PEACETIME project (http://peacetime-project.org), a joint initiative of the MERMEX and CHARMEX components supported by CNRS-INSU, IFREMER, CEA, and Météo-France as part of the program MISTRALS coordinated by INSU (doi.org/10.17600/17000300). Part of the dataset have been acquired during the PEACETIME oceanographic expedition on board R/V *Pourquoi Pas?* in May-June 2017.

This study is a contribution to the following research projects: NAOS (funded by the Agence Nationale de la Recherche in the frame of the French "Equipement d'Avenir" program, grant ANR J11R107-F), remOcean (funded by the European Research Council, grant 246777), and BGC-Argo France (funded by CNES-TOSCA and LEFE-GMMC).

We thank Sandra Helias Nunige, Joris Guittonneau and Patrick Raimbault for the sampling, analysis and inventory of nutrients during the cruise PEACETIME.

We thank the PIs of cruises MOOSE-GE, Laurent Coppola and Pierre Testor, the PI of the cruise VENUS2, Katrin Schroeder, and the PI of the cruise MEDSEA, Patrizia Ziveri, who allowed the deployment and recovery of the BGC-Argo floats. Captains and crew of R/V *Tethys II* (CNRS-INSU), R/V *Pourquoi Pas?* (Ifremer), R/V *Angeles Alvariño* (IEO) and *R/V Urania* (CNR) who participated to the deployments of the floats are also thanked.

We thank the International Argo Program and the CORIOLIS operational oceanography center that contribute to make the floats data freely and publicly available (doi.org/10.17882/42182).

References

Aminot, A., and Kerouel, R. : Dosage automatique des nutriments dans les eaux marines méthodes en flux continu, In: Méthodes d'analyse en milieu marin, Ifremer Editions, 25, Quae, 2007.

Astraldi, M., and Gasparini, G.P.: The seasonal characteristics of the circulation in the Tyrrhenian Sea. In: The seasonal and interannual variability of the western Mediterranean Sea, P. E. La Violette. editor. Coastal and Estuarine Studies, Vol. 46, Agu, Washington, pp. 115-134, 1994.

Astraldi, M., Conversano, F., Civitarese, G., Gasparini, G. P., Ribera d'Alcalà, M. and Vetrano, A.: Water mass properties and chemical signatures in the central Mediterranean region, Journal of Marine Systems, 33, 155-177, 2002.

Barbieux, M., Uitz, J., Gentili, B., Pasqueron de Fommervault, O., Mignot, A., Poteau, A., Schmechtig, C., Taillandier, V., Leymarie, L., Penkerc'h, C., D'Ortenzio, F., Claustre, C., and Bricaud, A.: Bio-optical characterization of subsurface chlorophyll maxima in the Mediterranean Sea from a Biogeochemical-Argo float database, Biogeosciences, 16, 1321-1342, 2019.

Béthoux, J.-P.: Oxygen consumption, new production, vertical advection and environmental evolution in the Mediterranean Sea, Deep Sea Research, 36, 769–781, 1989.

Béthoux, J.P., Morin, P., Chaumery, C., Connan, O., Gentili, B., and Ruiz-Pino, D.: Nutrients in the Mediterranean Sea, mass balance and statistical analysis of concentrations with respect to environmental change, Marine Chemistry, 63, 155-169, 1998.

Biogeochemical-Argo Planning Group: The Scientific Rationale, Design and Implementation Plan for a Biogeochemical-Argo Float Array (Report). Issy-les- Moulineaux: Ifremer, 2016.

Bouffard, D., and Boegman, L: A diapycnal diffusivity model for stratified environmental flows, Dynamics of Atmosphere and Oceans, 61-62, 14-34, 2013.

Bryden, H., Schroeder, K., Sparnocchia, S., Borghini, M., and Vetrano, A.: Thermohaline staircases in the western Mediterranean Sea, Journal of Marine Research, 72, 1–18, 2014.

Buffett, G.G., Krahmann, G., Klaeschen, D., Schroeder, K., Sallarès, V., Papenberg, C., Ranero, C.R., and Zitellini, N.: Seismic oceanography in the Tyrrhenian Sea: thermohaline staircases, eddies, and internal waves, Journal of Geophysical Research, 122, 2017.

Cotroneo, Y., Aulicino, G., Ruiz, S., Sánchez Román, A., Torner Tomàs, M., Pascual, A., Fusco, G., Heslop, E., Tintoré, J., and Budillon, G.: Glider data collected during the Algerian Basin Circulation Unmanned Survey, Earth System Science Data, 11, 147–161, 2019.

Cuypers, Y., Bouruet-Aubertot, P., Marec, C., and Fuda, J.L.: Characterization of turbulence from a fine-scale parameterization and microstructure measurements in the Mediterranean Sea during the BOUM experiment, Biogeosciences, 9, 3131-3149, 2012.

Dillon, T.M.: Vertical overturns: a comparison of Thorpe and Ozmidov length scales, Journal of Geophysical Research, 87, 9601-9613, 1982.

D'Ortenzio, F., and Ribera d'Alcalà, M.: On the trophic regimes of the Mediterranean Sea: a satellite analysis, Biogeosciences, 6, 139–148, 2009.

D'Ortenzio F., Taillandier, V., Claustre, H., Prieur, L., Leymarie, E., Mignot, A., Poteau, A., Penkerc'h, C., and Schmechtig, C.: Biogeochemical Argo: the test case of the NAOS Mediterranean array, Frontiers in Marine Science, 7:120, 2020.

Durante, S., Schroeder, K., Mazzei, L., Pierini, S., Borghini, M., and Sparnocchia, S.: Permanent thermohaline staircases in the Tyrrhenian Sea, Geophysical Research Letters, 46, 1562–1570, 2019.

Falco, P., Trani, M., and Zambianchi, E.: Water mass structure and deep mixing processes in the Tyrrhenian Sea: results from the VECTOR project, Deep Sea Research Part I, 113, 7-21, 2016.

Fernandez-Castro, B., Mourino-Carballido, B., Maranon, E., Choucino, P., Gago, J., Ramirez, T., Vidal, M., Bode, A., Blasco, D., Royer, S.J., Estrada, M., and Simo, R.: Importance of salt fingering for new nitrogen supply in the oligotrophic ocean, Nature Communications, 6, 8002, 2015.

Ferron, B., Bouruet Aubertot, P., Cuypers, Y., Schroeder, K., and Borghini, M.: How important are diapycnal mixing and geothermal heating for the deep circulation of the Western Mediterranean? Geophysical Research Letters, 44, 7845–7854, 2017.

Gasparini, G.P., Ortona, A., Budillon, G., Astraldi, M., and Sansone, E.: The effect of the Eastern Mediterranean Transient on the hydrographic characteristics in the strait of Sicily and in the Tyrrhenian Sea, Deep Sea Research Part I, 52, 915-935, 2005.

Guieu, C., D'Ortenzio, F., Dulac, F., Taillandier, V., Doglioli, A., Petrenko, A., Barrillon, S., Mallet, M., Nabat, P., and Desboeufs, K. : Process studies at the air-sea interface after atmospheric deposition in the Mediterranean Sea: objectives and strategy of the PEACETIME oceanographic campaign (May-June 2017). Biogeosciences, in revision for this special issue.

Guieu, C., and Desboeufs, K. : PEACETIME cruise, RV Pourquoi Pas ?, doi :10.17600/17000300, 2017.

Hamilton, J.M., Lewis, M.R., and Ruddick, B.R.: Vertical fluxes of nitrate associated with salt fingers in the world's oceans, Journal of Geophysical Research, 94, 2137–2145, 1989.

Jambu, M.: Fortran IV computer program for rapid hierarchical classification of large data sets, Computers & Geosciences, 7, 297-310, 1981.

Johnson, K. S., and Coletti, L. J.: In situ ultraviolet spectrophotometry for high resolution and long-term monitoring of nitrate, bromide and bisulfide in the ocean, Deep-Sea Res. Pt. I, 49, 1291– 1305, 2002.

Keraghel, M., Louanchi, F., Zerrouki, M., Ait Kaci, M., Aït-Ameur, N., Labaste, M., Legoff, H., Taillandier, V., Harid, R., and Mortier, L.: Carbonate system properties and anthropogenic carbon inventory in the Algerian Basin during SOMBA cruise (2014): acidification rate estimate, Marine Chemistry, doi.org/10.1016/j.marchem.2020.103783, 2020.

Krahmann, G.: Horizontal variability of thermohaline staircases in the western Mediterranean, Double-Diffusive Processes, 1996 Summer Study Program in Geophysical Fluid Dynamics, S. Meacham and D. Tucholke, Eds., Woods Hole Oceanographic Institution, Technical Report WHOI-97-10, 331–347, 1997.

Kress, N., Manca, B.B., Klein, B., and Deponte, D.: Continuing influence of the changed thermohaline circulation in the eastern Mediterranean on the distribution of dissolved oxygen and nutrients: Physical and chemical characterization of the water masses, Journal of Geophysical Research Oceans, 108, 8109, 2003.

Krivosheya, V.G., and Ovchinnikov, I.M.: Pecularities in the geostrophic circulation of the waters of the Tyrrhenian Sea, Oceanology, 13, 822-827, 1973.

Large, W.G., McWilliams, J.C., and Doney, S.C.: Oceanic vertical mixing: a review and a model with a nonlocal boundary layer parameterization. Review of Geophysics, 32, 363–403, 1994.

Lascaratos, A., Roether, W., Nittis, K., and Klein, B.: Recent changes in deep water formation and spreading in the eastern Mediterranean Sea: a review, Progress in Oceanography, 44, 5-36, 1999.

Lavigne, H., D'Ortenzio, F., Migon, C., Claustre, H., Testor, P., Ribera d'Alcalà, M., Lavezza, R., Houpert, L., and Prieur, L.: Enhancing the comprehension of mixed layer depth control on the Mediterranean phytoplankton phenology, Journal of Geophysical Research, 118, 3416-3430, 2013.

Mallil, K., Testor, P., Le Goff, H., Mortier, L., Taillandier, V., Ait Ameur, N., Louanchi, F., and Labaste, M. : Hydrologie et circulation océanique dans le gyre est et ouest du bassin Algérien, Rapport de la Commission Internationale de la Mer Méditerranée, 41, 86, 2016.

Malanotte-Rizzoli, P., Manca, B.B., Marullo, S., Ribera d'Alcalà, M., Roether, W., Theocharis, A., and Conversano, F.: The Levantine Intermediate Water Experiment (LIWEX) Group: Levantine basin - A laboratory for multiple water mass formation processes, Journal of Geophysical Research Oceans, 108, 2003.

McDougall, T.J.: Double-diffusive interleaving. Part II: finite amplitude, steady state interleaving, Journal of Physical Oceanography, 15, 1542-1556, 1985.

MEDOC Group: Observation of Formation of Deep Water in the Mediterranean Sea, 1969, Nature, 227, 1037, 1970.

Merryfield, W.J.: Origin of thermohaline staircases, Journal of Physical Oceanography, 30, 1046–1068, 2000.

Molcard, R., and Tait, R.I.: The steady state of the step structure in the Tyrrhenian Sea, In: A voyage of discovery: George Deacon seventieth anniversary volume, M. Angel, editor, Pergamon Press, New York, pp. 221-233, 1977.

Morel, A., and André, J.M.: Pigment distribution and primary production in the western Mediterranean as derived and modeled from coastal zone color scanner observations, Journal of Geophysical Research Oceans, 96, 12685-12698, 1991.

Mortier, L., Aït Ameur, N., and Taillandier, V. : SOMBA-GE-2014 cruise, RV Téthys II, doi:10.17600/14007500, 2014.

Mouriño-Carballido, B., Hojas, E., Cermeño, P., Chouciño, P., Fernández-Castro, B., Latasa, M., Marañón, E., Morán, X.A.G., and Vidal, M.: Nutrient supply controls picoplankton community structure during three contrasting seasons in the northwestern Mediterranean Sea, Marine Ecology Progress Series, 543, 1-19, 2016.

Nittis, K., and Lascaratos, A.: Intermediate water formation in the Levantine Sea: the response to interannual variability of atmospheric forcing, In: The eastern Mediterranean as a laboratory basin for the assessment of contrasting ecosystems (pp. 441-446). Springer, Dordrecht, 1999.

Omand, M.M., and Mahadevan, A.: The shape of the oceanic nitracline, Biogeosciences, 12, 3273–3287, 2015.

Onken, R., and Brembilla E.: Double diffusion in the Mediterranean Sea: observation and parameterization of salt finger convection, Journal of Geophysical Research, 108, 8124, 2003.

Osborn, T.R.: Estimates of local rate of vertical diffusion from dissipation measurements, Journal of Physical Oceanography 10, 83–89, 1980.

Park, Y. H., Lee, J. H., Durand, I., and Hong, C. S.: Validation of Thorpe-scale-derived vertical diffusivities against microstructure measurements in the Kerguelen region. Biogeosciences, 11, 6927–6937, 2014.

Pasqueron de Fommervault, O., D'Ortenzio, F., Mangin, M., Serra, R., Migon, C., Claustre, H., Lavigne, H., Ribera d'Alcalà, M., Prieur, L., Taillandier, V., Schmechtig, C., Poteau, A., Leymarie, E., Besson, F., and Obolensky, G.: Seasonal variability of nutrient concentrations in the Mediterranean Sea: Contribution of Bio-Argo floats, Journal of Geophysical Research Oceans, 120, 2015.

Poulain, P.M., Barbanti, R., Font, J., Cruzado, A., Millot, C., Gertman, I., Griffa, A., Molcard, A., Rupolo, V., Le Bras, S., and Petit de la Villeon, L.: MedArgo: a drifting profiler program in the Mediterranean Sea, Ocean Science, 3, 379- 395, 2007.

Prieur, L., Béthoux, J.P., Bong, J.H., and Taillez, D. : Particularités hydrologiques et formation d'eau profonde dans le bassin Liguro-Provençal en 1981-1982, Rapport de la Commission Internationale de la Mer Méditerranée, 28, 51-53, 1983.

Pujo-Pay, M., Conan, P., Oriol, L., Cornet-Barthaux, V., Falco, C., Ghiglione, J.F., Goyet, C., Moutin, T., and Prieur, L.: Integrated survey of elemental stoichiometry (C, N, P) from the western to eastern Mediterranean Sea, Biogeosciences, 8, 883-899, 2011.

Radko, T.: What determines the thickness of layers in a thermohaline staircase? Journal of Fluid Mechanics, 523, 79-98, 2005.

Radko, T., and Smith, D.P.: Equilibrium transport in double-diffusive convection, Journal of Fluid Mechanics, 692, 5–27, 2012.

Radko, T., Flanagan, J.D., Stellmach, S., and Timmermans, M.L.: Double-diffusive recipes. Part 2: Layer-merging events, Journal of Physical Oceanography, 44, 1285-1305, 2014.

Ribera d'Alcalà, M., Civitarese, G., Conversano, F., and Lavezza, R.: Nutrient ratios and fluxes hint at overlooked processes in the Mediterranean Sea, Journal of Geophysical Research Oceans, 108, 8106, 2003.

Roether, W., Klein, B., Manca, B.B., Theocharis, A., and Kioroglou, S.: Transient Eastern Mediterranean deep waters in response to the massive dense-water output of the Aegean Sea in the 1990s, Progress in Oceanography, 74, 540-571, 2007.

Send, U., and Testor, P.: Direct observations reveal the deep circulation of the western Mediterranean Sea, Journal of Geophysical Research Oceans, 122, 2017.

Sakamoto, C. M., Johnson, K. S., and Coletti, L. J.: Improved algorithm for the computation of nitrate concentrations in sea-water using an in situ ultraviolet spectrophotometer, Limnology and Oceanography-Methods, 7, 132–143, 2009.

Santolleri, C., Iacono, R., Napolitano, E., and Ribera d'Alcalá, M.: Surface transport of DOC acts as a trophic link among Mediterranean sub-basins, Biogeosciences Discussion, doi.org/10.5194/bg-2018-418, 2018.

Schmitt, R.W.: Form of the temperature-salinity relationship in the Central Water: evidence for double-diffusive mixing, Journal of Physical Oceanography, 11, 1015-1026, 1981.

Schmitt, R.W.: Double diffusion in oceanography. Annual Review of Fluid Mechanics, 26, 255–285, 1994.

Schmitt, R.W., Perkins, H., Boyd, J.D., and Stalcup, C.: C-SALT: an investigation of the thermohaline staircase in the western tropical North Atlantic, Deep Sea Research, 34, 1655-1665, 1987.

Sparnocchia, S., Gasparini, G.P., Astraldi, M., Borghini, M., and Pistek, P.: Dynamics and mixing of the Eastern Mediterranean outflow in the Tyrrhenian basin, Journal of Marine Systems, 20, 301–317, 1999.

Stern, M.E.: The "Salt-Fountain" and Thermohaline Convection, Tellus, 12:2, 172-175, 1960.

Stern, M.E., and Turner, J.S.: Salt fingers and convecting layers, Deep Sea Research, 16, 497–511, 1969.

Taillandier, V., Wagener, T., D'Ortenzio, F., Mayot, N., Legoff, H., Ras, J., Coppola, L., Pasqueron de Fommervault, O., Schmechtig, C., Diamond, E., Bittig, H., Lefevre, D., Leymarie, E., Poteau, A., and Prieur, L.: Hydrography and biogeochemistry dedicated to the Mediterranean BGC-Argo network during a cruise with RV Tethys 2 in May 2015, Earth System Science Data, 10, 1–15, 2018.

Testor, P., and Gascard, J.C.: Large scale flow separation and mesoscale eddy formation in the Algerian Basin, Progress in Oceanography, 66, 211–230, 2005.

Testor, P., Send, U., Gascard, J.C., Millot, C., Taupier-Letage, I., and Beranger, K.: The mean circulation of the southwestern Mediterranean Sea: Algerian Gyres, Journal of Geophysical Research, 110, C110017, 2005.

Testor, P., Le Goff, H., Labaste, M., Coppola, L., Mortier, L., Taillandier, V., Dausse, D., Kunesch, S., Diamond-Riquier, E., Garcia, N., Durrieu de Madron, X., and Raimbault, P. : MOOSE-GE, doi:10.18142/235, 2010.

Williams, R.G., and Follows, M.J.: Physical transport of nutrients and the maintenance of biological production, In: Fasham M.J.R. (eds) Ocean Biogeochemistry, Global Change - The IGBP Series, Springer, Berlin, Heidelberg, 2003.

Wong, A., Keeley, R., Carval, T., and the Argo Data Management Team: Argo Quality Control Manual for CTD and Trajectory Data, doi:10.13155/33951, 2019.

Wüst, G.: On the vertical circulation of the Mediterranean Sea, Journal of Geophysical Research, 66, 10, 1961.

Ziveri, P., and Grelaud, M.: Physical oceanography during Ángeles Alvariño cruise MedSeA2013, Universitat Autònoma de Barcelona, PANGAEA, doi:10.1594/PANGAEA.846067, 2015.

Zodiatis, G., and Gasparini, G.P.: Thermohaline staircase formations in the Tyrrhenian Sea, Deep Sea Research Part I, 43, 655–678, 1996.

Zunino, P., Schroeder, K., Vargas-Yáñez, M., Gasparini, G.P., Coppola, L., García-Martínez, M.C., and Moya-Ruiz, F.: Effects of the Western Mediterranean Transition on the resident water masses: pure warming, pure freshening and pure heaving, Journal of Marine Systems, 96-97, 15-23, 2012.

Float WMO	First profile	Last profile	Algerian Basin	Tyrrhenian Sea
6901513	09 May 2013 - 0	16 Jun 2015 - 182	116 / 183 (63%)	/
6901600	23 Aug 2014 - 1	23 Dec 2015 - 101	92 / 102 (90%)	/
6902732	16 Jan 2017 - 41	18 Dec 2017 - 91	16 / 51 (31%)	/
6901491	16 Jun 2013 - 0	30 May 2015 - 178	/	152 / 179 (85%)
6901769	31 May 2015 - 0	02 May 2017 - 143	/	102 / 144 (71%)
TOTAL	09 May 2013	18 Dec 2017	224 / 336 (67%)	254 / 323 (79%)

Table 1: Selection of CTD profiles collected by five floats operated in the Algerian Basin and in the Tyrrhenian Sea. Each deployment is labeled by the float Word Meteorological Organization (WMO) number. Date and cycle number of the first and the last profiles of this selection, number of profiles (with staircase detection / total, proportion in %).

Depth Interval (dbar)	ε (10^{-9} W/kg)	K_{turb} (10^{-5} m^2/s)
20 – 100	6 – 10 *	
100 – 150	7.7 +/- 10.4	3.5 +/- 4.8
150 – 200	4.6 +/- 4.6	6.0 +/- 6.0
200 – 250	4.7 +/- 4.4	11.0 +/- 10.2
250 – 300	3.1 +/- 1.7	14.0 +/- 7.9
300 – 350	3.1 +/- 2.3	24.4 +/- 18.3
350 – 400	0.9 +/- 0.3	9.6 +/- 3.0

Table 2: look-up table for turbulent kinetic energy dissipation rates and vertical eddy diffusivity derived from a Thorpe-scale based parameterization, and applied to the full-resolution CTD profiles of the cruise PEACETIME collected in the Algerian Basin and in the central Tyrrhenian Sea. The methodological approach described by Park et al. (2014) has been strictly followed, by averages by 50m bins over the 13 profiles represented in Figures 3 and 7. For surface values (*), the range of estimation proposed by Cuypers et al. (2012) is used.

Layer	Depth interval (dbar) Top	Bottom	Layer Thickness (dbar)	Layer Temperature (°C)	Layer Salinity	Interface Thickness (dbar)	Interface Temperature Difference (°C)	Interface Salinity Difference	Density Ratio
1	614 +/- 3	660 +/- 1	46 +/- 2	13.862 +/- 0.000	38.720 +/- 0.000				
						4 +/- 1	0.079 +/- 0.000	0.017 +/- 0.000	1.38 +/- 0.03
2	664 +/- 2	728 +/- 3	64 +/- 3	13.784 +/- 0.001	38.703 +/- 0.000				
						14 +/- 4	0.134 +/- 0.001	0.031 +/- 0.000	1.32 +/- 0.03
3	741 +/- 6	821 +/- 8	80 +/- 9	13.650 +/- 0.001	38.672 +/- 0.000				
						6 +/- 2	0.096 +/- 0.001	0.022 +/- 0.000	1.31 +/- 0.03
4	827 +/- 8	956 +/- 8	129 +/- 5	13.554 +/- 0.001	38.650 +/- 0.000				
						28 +/- 6	0.192 +/- 0.001	0.047 +/- 0.000	1.26 +/- 0.01
5	983 +/- 3	1259 +/- 15	276 +/- 14	13.362 +/- 0.000	38.603 +/- 0.000				
						56 +/- 10	0.147 +/- 0.001	0.038 +/- 0.000	1.20 +/- 0.00
6	1314 +/- 7	1647 +/- 8	332 +/- 1	13.216 +/- 0.000	38.565 +/- 0.000				
						40 +/- 9	0.063 +/- 0.001	0.018 +/- 0.000	1.14 +/- 0.03
7	1687 +/- 7	1871 +/- 5	184 +/- 8	13.153 +/- 0.000	38.547 +/- 0.000				
						78 +/- 8	0.054 +/- 0.001	0.015 +/- 0.000	1.16 +/- 0.03
8	1948 +/- 9	2033 +/- 20	85 +/- 13	13.099 +/- 0.000	38.532 +/- 0.000				
						35 +/- 15	0.022 +/- 0.000	0.006 +/- 0.000	1.20 +/- 0.02
9	2067 +/- 8	2167 +/- 17	100 +/- 14	13.077 +/- 0.000	38.526 +/- 0.000				
						32 +/- 16	0.021 +/- 0.000	0.007 +/- 0.000	1.19 +/- 0.03
10	2199 +/- 8	2275 +/- 18	76 +/- 17	13.056 +/- 0.000	38.519 +/- 0.000				

Table 3: Characteristics of the staircases in the Tyrrhenian Sea, extracted from the four casts of the cruise PEACETIME (Figure 3). The layers are selected thicker than 15 dbar, the layer numbering is incremented downwards. Parameters are presented as average value and standard deviation over the four casts.

Layer	Depth interval (dbar)		Layer Thickness (dbar)	Layer Temperature (°C)	Layer Salinity	Interface Thickness (dbar)	Interface Temperature Difference (°C)	Interface Salinity Difference	Density Ratio
1	611 +/- 21	636 +/- 17	25 +/- 8	13.249 +/- 0.003	38.555 +/- 0.001				
						33 +/- 6	0.062 +/- 0.002	0.013 +/- 0.001	1.42 +/- 0.04
2	669 +/- 18	713 +/- 15	44 +/- 10	13.188 +/- 0.001	38.542 +/- 0.000				
						32 +/- 8	0.054 +/- 0.002	0.012 +/- 0.001	1.37 +/- 0.05
3	744 +/- 21	807 +/- 13	63 +/- 12	13.133 +/- 0.002	38.530 +/- 0.001				
						48 +/- 13	0.072 +/- 0.001	0.016 +/- 0.000	1.31 +/- 0.02
4	850 +/- 16	923 +/- 8	74 +/- 15	13.061 +/- 0.002	38.514 +/- 0.000				
						41 +/- 12	0.030 +/- 0.001	0.007 +/- 0.001	1.23 +/- 0.09
5	965 +/- 12	999 +/- 4	35 +/- 11	13.031 +/- 0.003	38.507 +/- 0.001				
						35 +/- 9	0.039 +/- 0.001	0.009 +/- 0.001	1.25 +/- 0.06
6	1034 +/- 9	1101 +/- 23	67 +/- 25	12.992 +/- 0.001	38.498 +/- 0.001				
						45 +/- 26	0.034 +/- 0.002	0.008 +/- 0.001	1.24 +/- 0.07
7	1154 +/- 13	1193 +/- 30	39 +/- 29	12.957 +/- 0.003	38.489 +/- 0.001				

Table 4: Characteristics of the staircases in the Algerian basin, extracted from the nine casts of the cruise PEACETIME (Figure 7). The layers are selected thicker than 15 dbar, the layer numbering is incremented downwards. Parameters are presented as average value and standard deviation over the nine casts.

Layer	All datasets May 2013 – Dec 2017	Inside box (37°20'N-38°N, 4°E-6°E)	Float 6901513 Sep 2013 – Dec 2013	Float 6901600 Nov 2014 – Apr 2015
1	0.78	0.82	0.89	0.91
2	0.77	0.83	0.90	0.98
3	0.73	0.83	0.93	0.94
4	0.67	0.76	0.90	0.89
5	0.65	0.74	0.91	0.82
AVERAGE	0.72	0.80	0.91	0.91

Table 5: lateral density ratios (R_L^i, Equation 3) defined by the changes of temperature and salinity within each layer (i). The average value over the five considered layers is reported. Ratios computed considering the whole dataset (Figure 12, upper left panel), the selection inside the box (37°20'N-38°N, 4°E-6°E) (Figure 12, upper right panel), and the two episodes (Figure 12, lower panels).

		Depth interval (dbar)	Density interval	Nitrate interval (µmol/kg)	Nitrate gradient (µmol/m^4)	ε (10^{-9} W/kg)	K_{sf} (10^{-5} m^2/s)	F_{NO3} (µmol/m^2/d)	Formulation
TYRRHENIAN SEA	Upper Nitracline	60 – 100	28.55 – 28.65	0 – 3.5	87.5	6 – 10		420 – 700	Eq. (8)
	Lower Nitracline	100 – 250	28.65 – 29.01	3.5 – 6.3	18.6	4.7 – 7.7		73 – 120	Eq. (8)
	Above LIW	250 – 400	29.01 – 29.07	6.3 – 6	-2	0.9 – 3.1		-31 – -9	Eq. (8)
	Below LIW	400 – 2000		6 – 8.3	1.4	-	1.5	1.9	Eq. (9)
	Below LIW	400 – 2000		6 – 8.3	1.4	-	3.3	4.0	Eq. (10)
	Below LIW	400 – 2000		6 – 8.3	1.4	-	6.7	8.3	Eq. (11)
ALGERIAN BASIN	Upper Nitracline	(70, 80) – 150	(28.08, 28.2) – 28.65	0 – 3.5	43.7 – 50	6 – 10		70 – 118 *	Eq. (8)
	Above LIW	150 – 350	28.65 – 29.03	3.5 – 10.1	33	3.1 – 4.6		108 – 160	Eq. (8)
	Below LIW	500 – 1500		9.7 – 9	-0.7	-	0.7	-0.2	Eq. (9)
	Below LIW	500 – 1500		9.7 – 9	-0.7	-	3.0	-1.8	Eq. (10)
	Below LIW	500 – 1500		9.7 – 9	-0.7	-	5.5	-3.3	Eq. (11)

* using $\partial C/\partial \rho$ computed by a linear regression of nitrate-density diagram within the density interval

Table 6: estimates of the nitrate fluxes in the central Tyrrhenian Sea and the Algerian Basin in presence of thermohaline staircases. Above LIW, the depth, density and nitrate intervals have been chosen to characterize well-defined segments from the nitrate dataset collected during the cruise PEACETIME (Figure 14, left panel). The ranges of the dissipation rates were extracted from the look-up Table 2. Note the linear regression to account for the fluctuations of the nitracline depth in the Algerian stations. Below LIW, the three formulations of the salt finger diffusivities in the transition zones have been applied with density ratios of 1.38 in the Algerian Basin and 1.32 in the Tyrrhenian Sea.

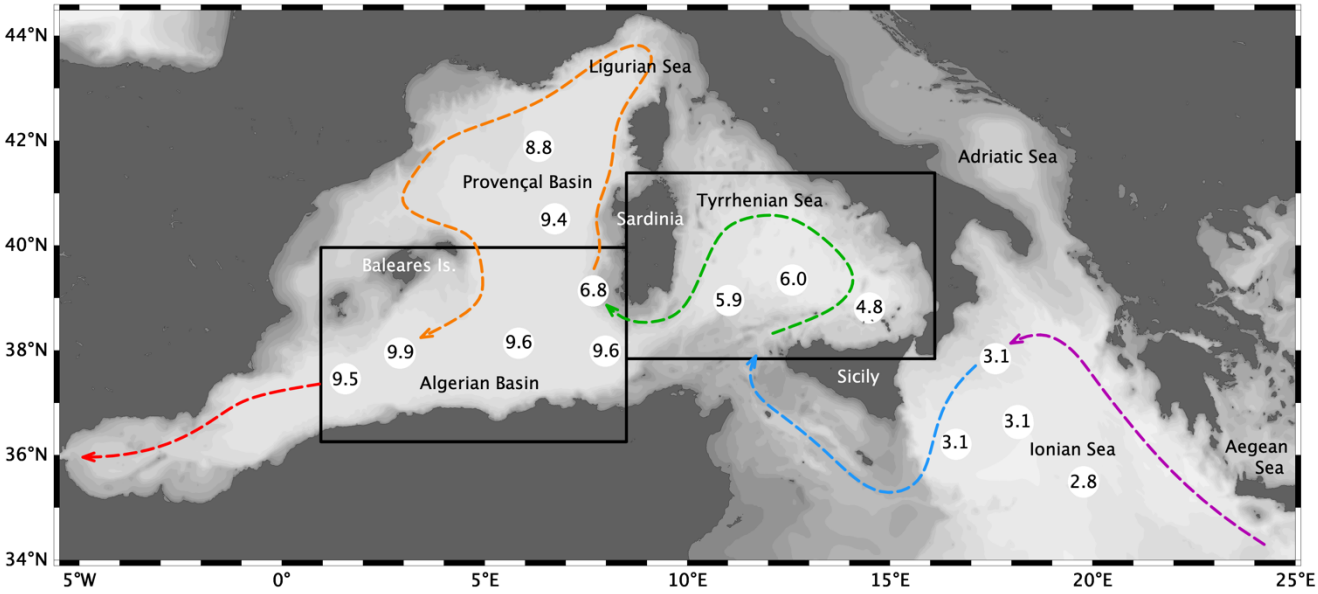

Figure 1: Indicative pathway of LIW in the western Mediterranean (dash line), crossing the two geographical areas under study (black boxes). Further analyzed in Section 3.3, nitrate concentrations (in µmol/kg) in LIW (immersion of the salinity maximum) as measured during the cruise PEACETIME.

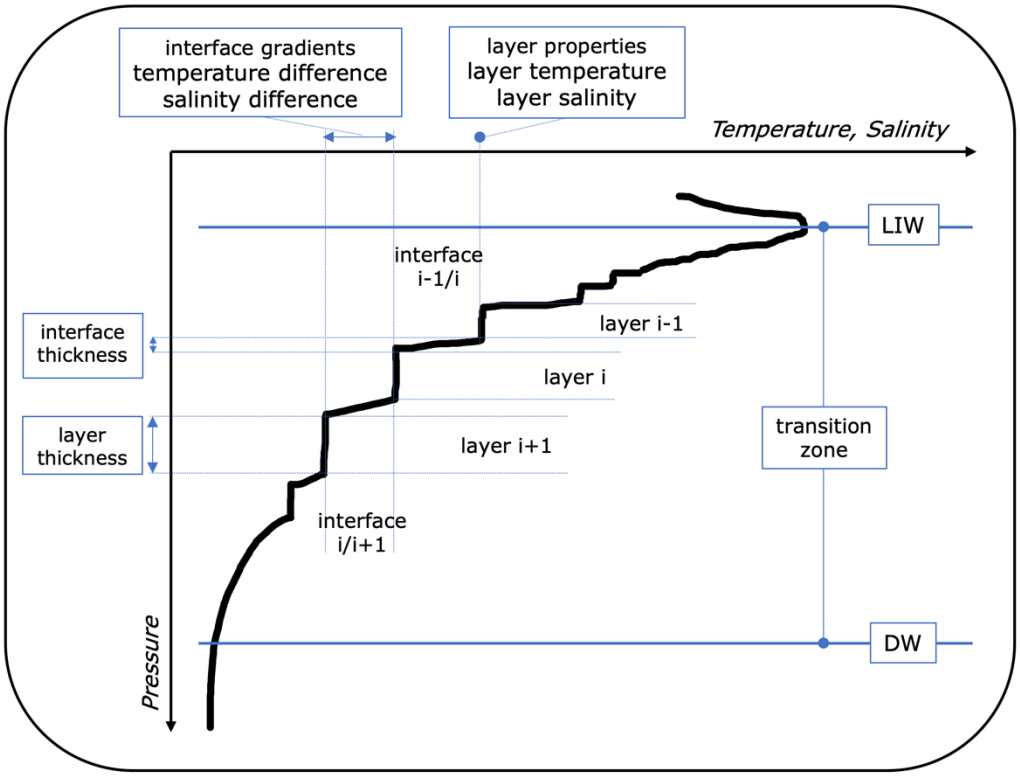

860 **Figure 2: Drawing of typical thermohaline staircases. Terminology used in the study to characterize the vertical structure. The layer number (i) and the interface number (i/i+1) are incremented downwards.**

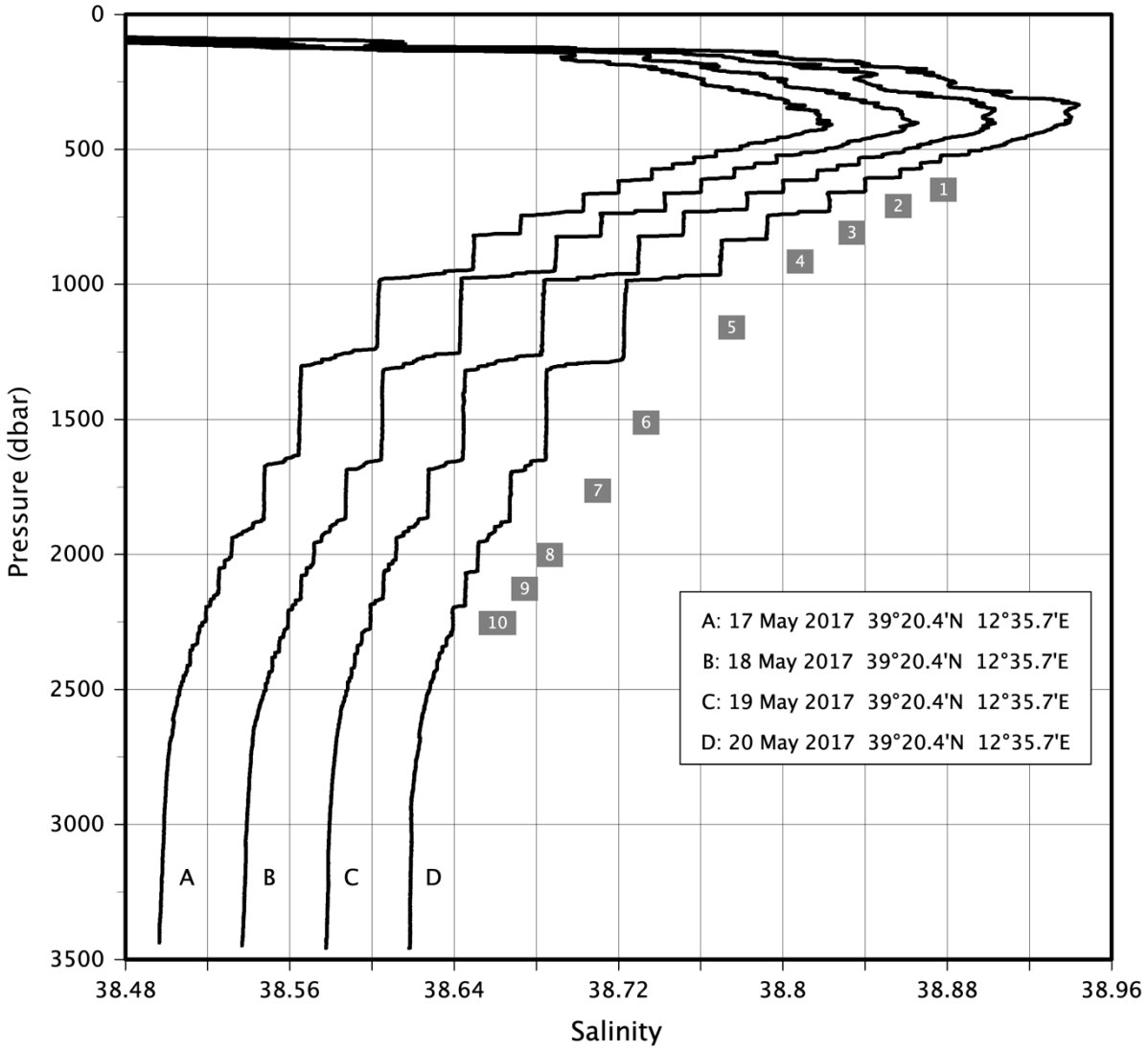

Figure 3: Sequence of daily salinity profiles observed in the Tyrrhenian Sea during the cruise PEACETIME. The four casts were performed from the surface to the bottom at the same location. The salinity scale is correct for the profile A and each subsequent profile is offset by 0.04. The layer numbering of Table 3 is indicated by grey boxes at average layer depths.

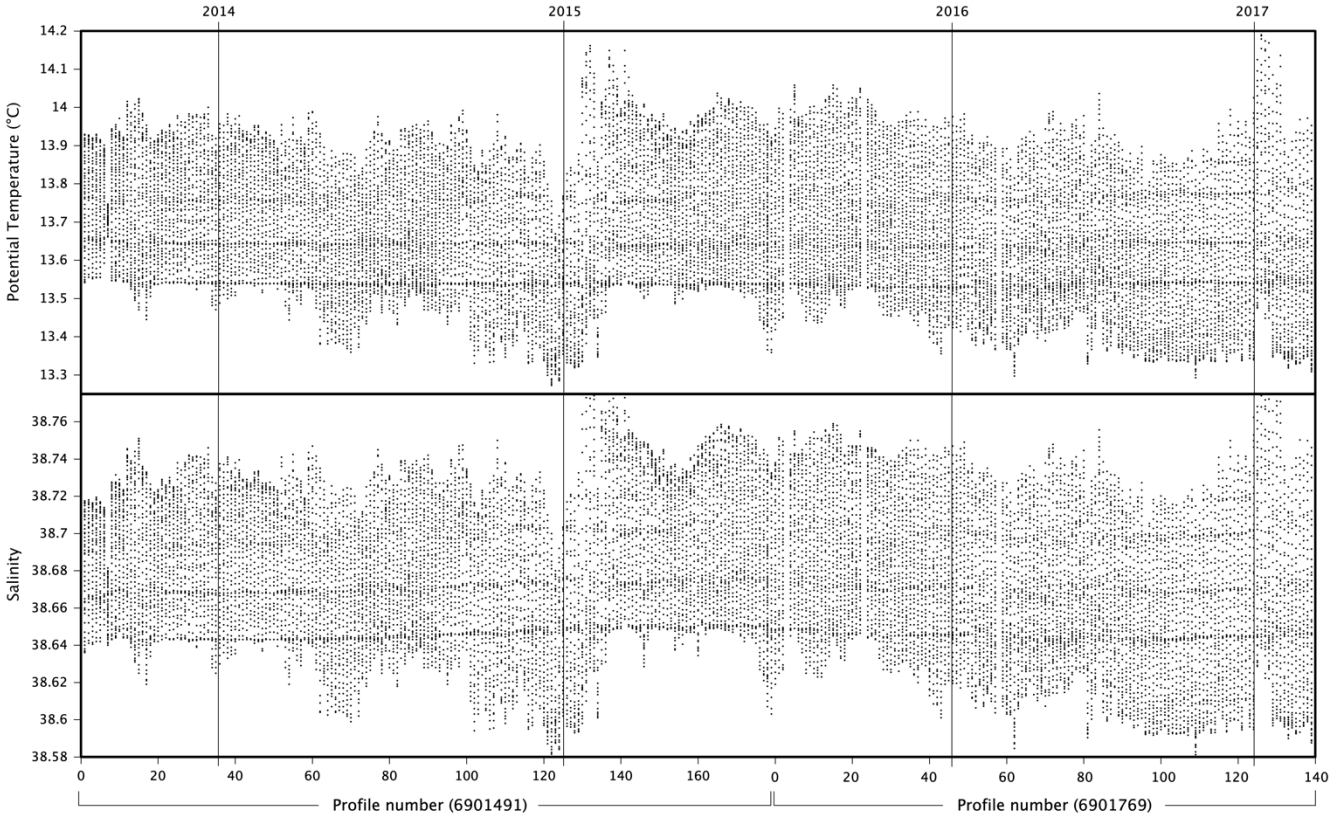

865

Figure 4: Temperature (upper panel) and salinity (lower panel) recorded in the range 300-1000 dbar with a vertical resolution of 10 dbar, by the consecutive deployments of the floats 6901491 and 6901769 in the Tyrrhenian Sea. In x-axis, the number of successive profiles with a resolution of one to seven days. The timeframe (in years) is superimposed by vertical lines.

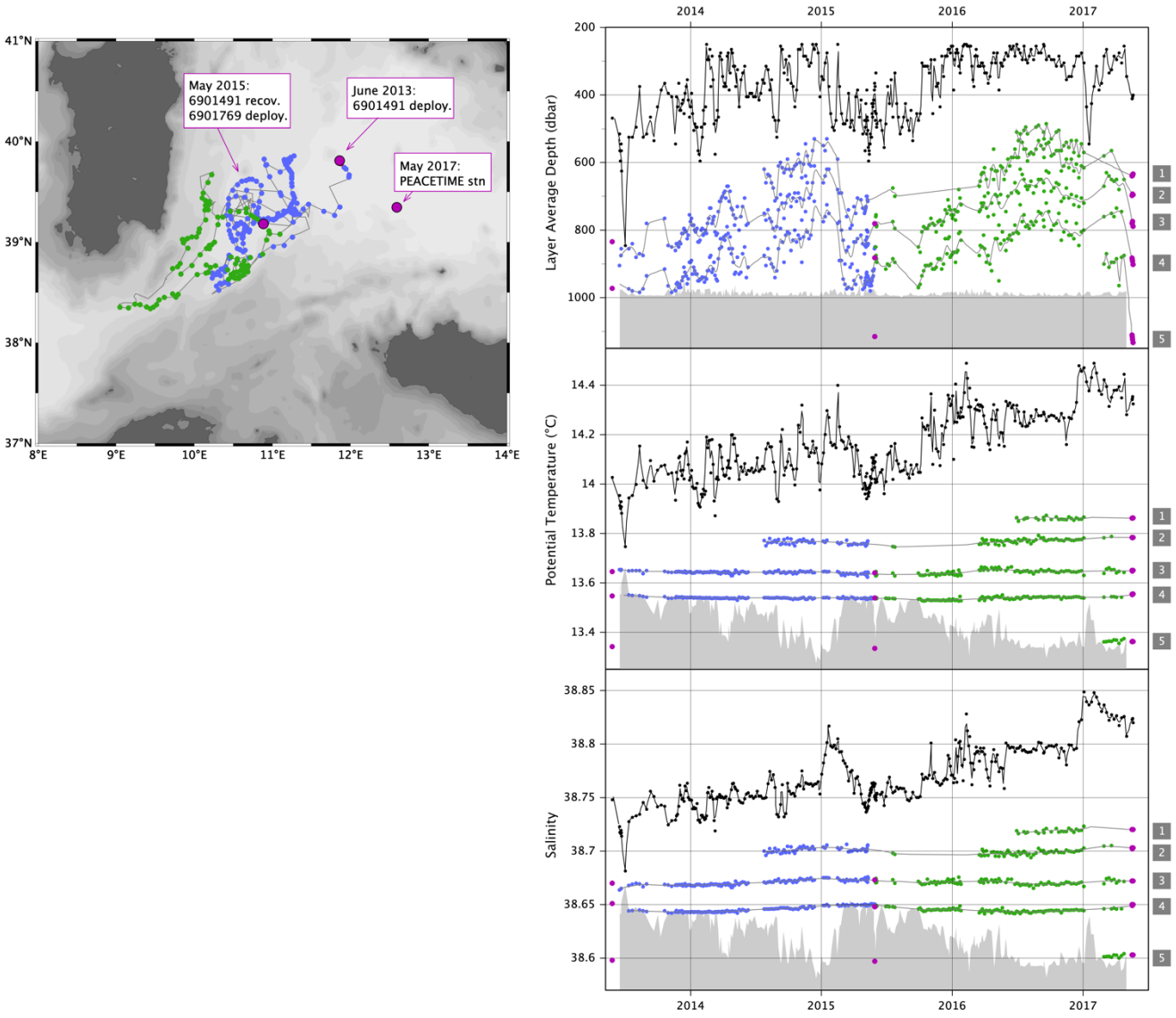

Figure 5: Left panel, location of staircase detections along the trajectory of the consecutive floats deployed in June 2013 and May 2015. Right panels, time series of layer properties and depth (colored dots) of shipboard and float profiles with staircase detection. LIW properties and depth are indicated in black lines. The 1000 dbar limit is indicated in grey shadows. The layer numbering of the station PEACETIME (Table 3) is indicated inside grey boxes. All panels: station locations and layer properties are indicated in purple for shipboard profiles, in blue for the float 6901491 and in green for the float 6901769.

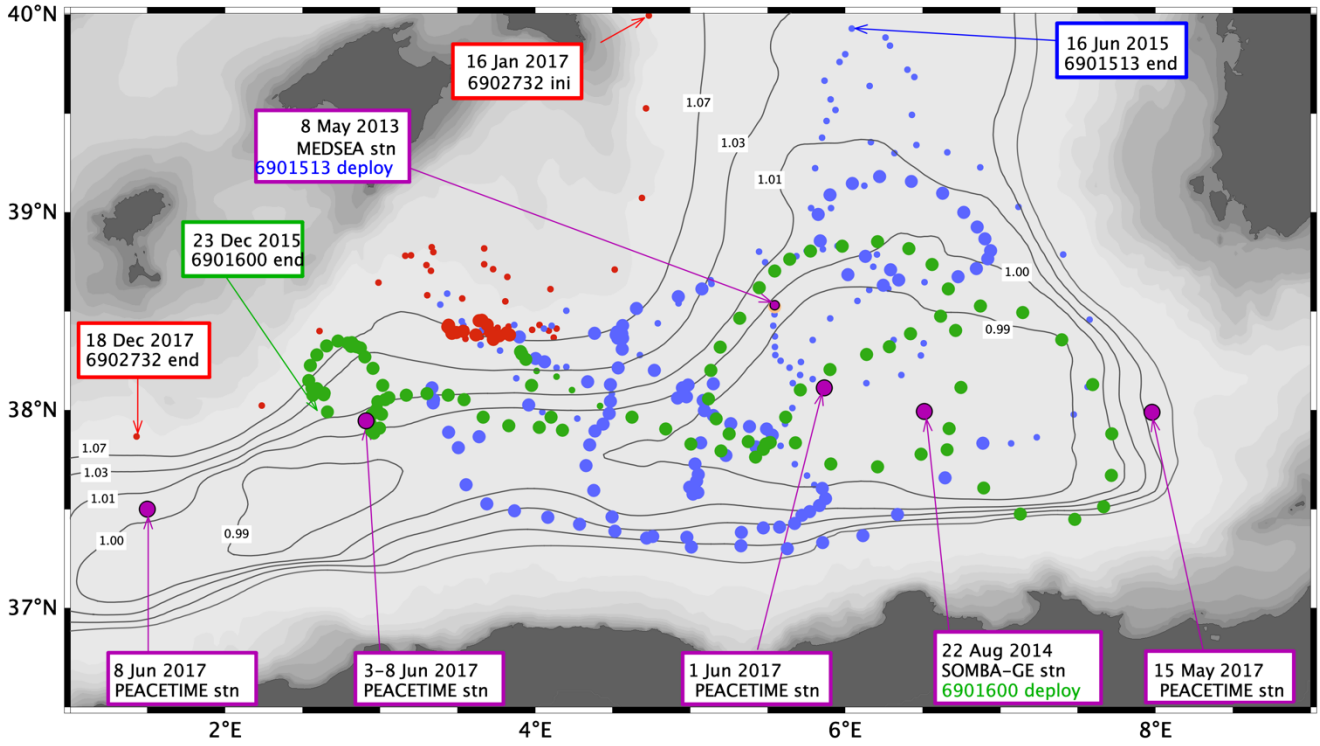

Figure 6: Locations of the CTD profiles in the Algerian Basin, in large or small dots whether or not staircases were detected. Float collections in blue for 6901513, in green for 6901600, in red for 6902732. Shipboard stations of float deployments and of the cruise PEACETIME in purple. Thin black lines: contours f/H normalized by f_o at 37°45'N and H_o = 2800 m.

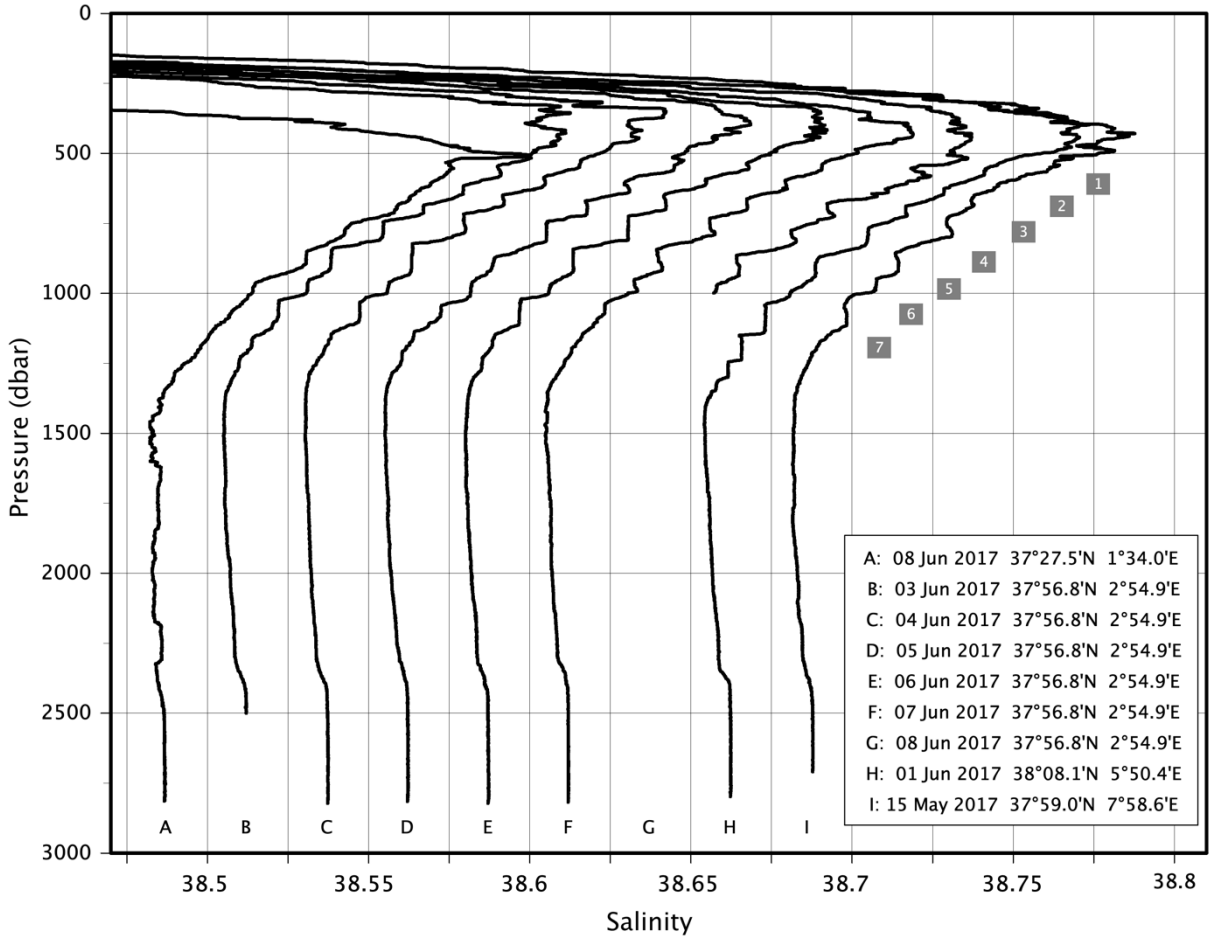

Figure 7: Sequence of salinity profiles along a zonal transect of four stations across the Algerian Basin during the cruise PEACETIME. The second station was repeated 6 times (casts B-G). The casts were performed from the surface to the bottom, unless cast B down to 2500 dbar and cast G down to 1000 dbar. The salinity scale is correct for the profile A and each subsequent profile is offset by 0.025. The layer numbering of Table 4 is indicated by grey boxes at average layer depths.

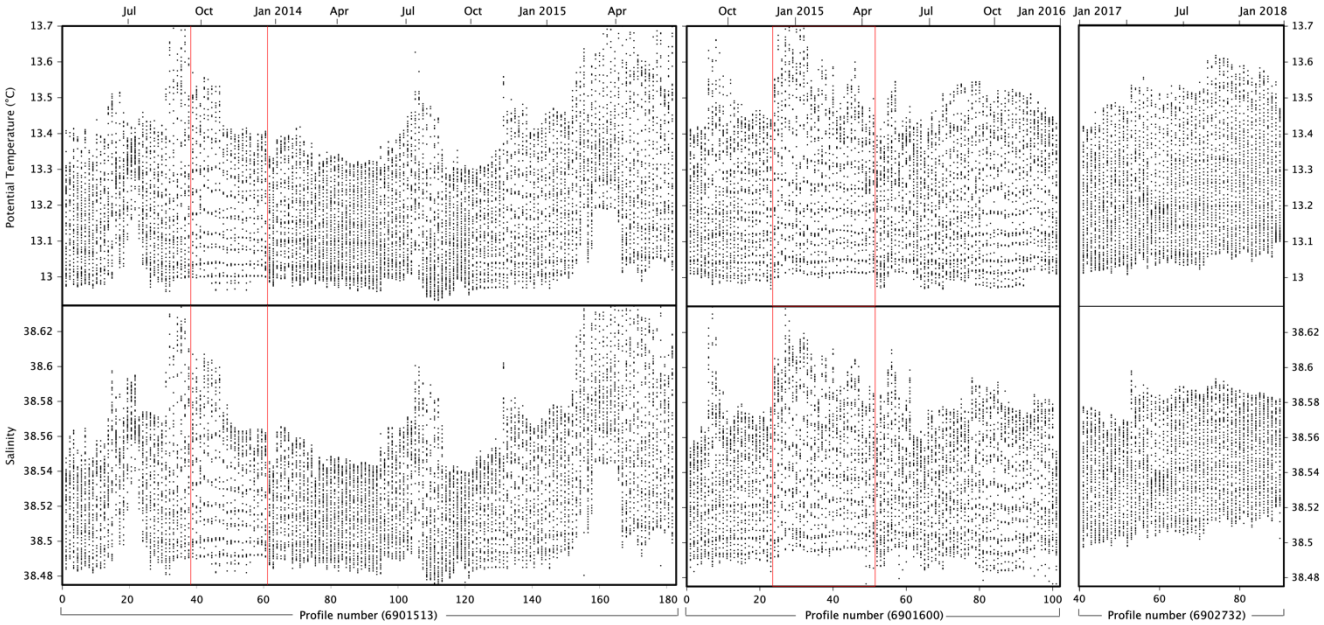

Figure 8: Temperature (upper panels) and salinity (lower panels) recorded in the range 300-1000 dbar with a vertical resolution of 10 dbar, by the three floats 6901513 (left panels), 6901600 (middle panels) and 6902732 (right panels) deployed in the Algerian Basin. In x-axis, number of the successive profiles with a resolution of one to seven days. The timeframe (in trimesters) is superimposed on top x-axis. The two episodes detailed in Section 3.2 are delimited by red lines.

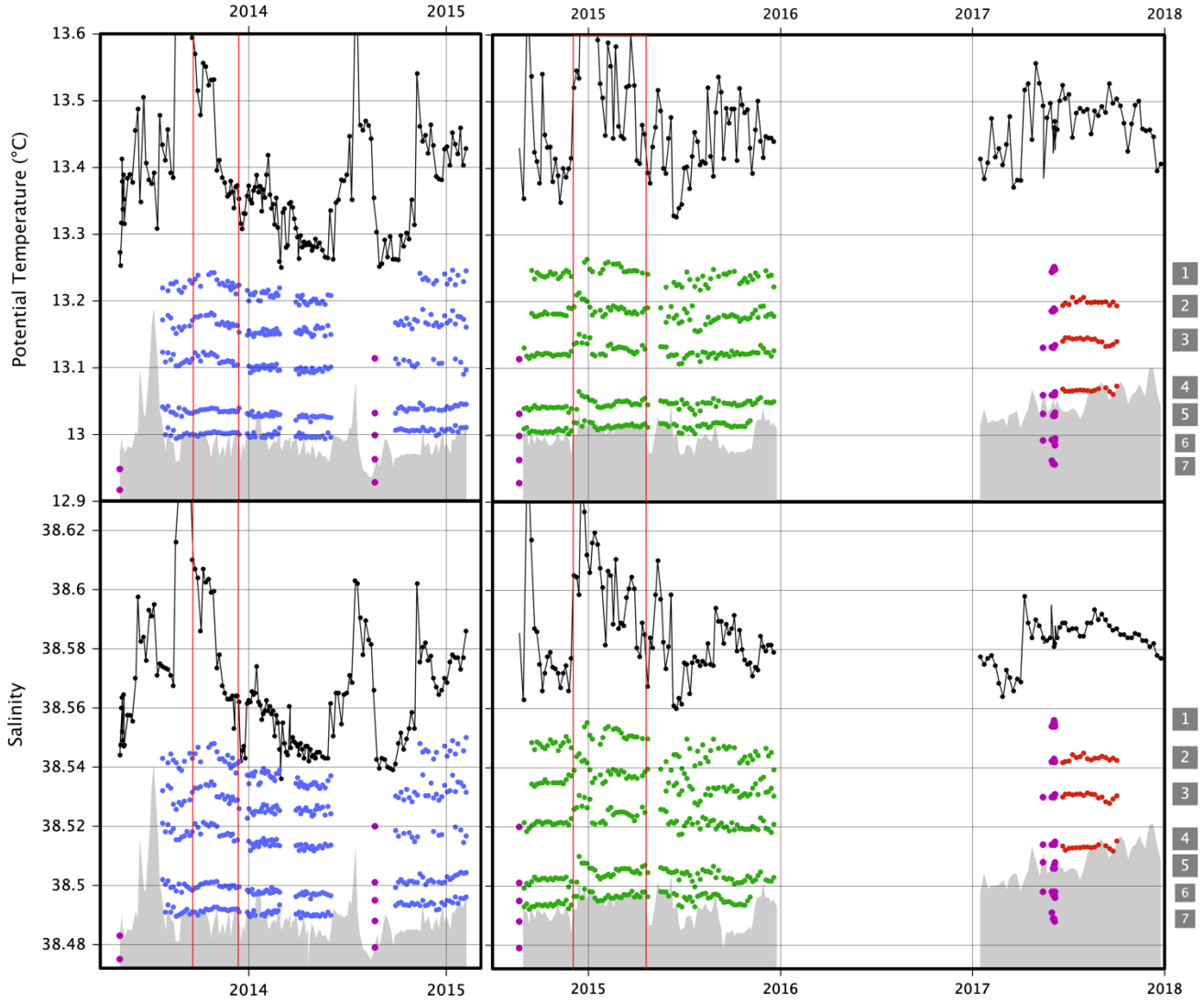

Figure 9: Time series of layer properties and depth (colored dots) of shipboard and float profiles with staircase detection, for temperature (upper panel) and salinity (lower panel). LIW properties and depth are indicated in black lines. The shipboard CTD profiles are indicated in purple, the float CTD profiles in blue (6901513), green (6901600) and red (6902732). The 1000 dbar limit is indicated by grey shadows. Time series of floats 6901513 and 6901600 are represented in distinct panels to avoid overlapping. The layer numbering of the stations PEACETIME (Table 4) is indicated by grey boxes in the right y-axis. The two episodes detailed in Section 3.2 are delimited by red lines.

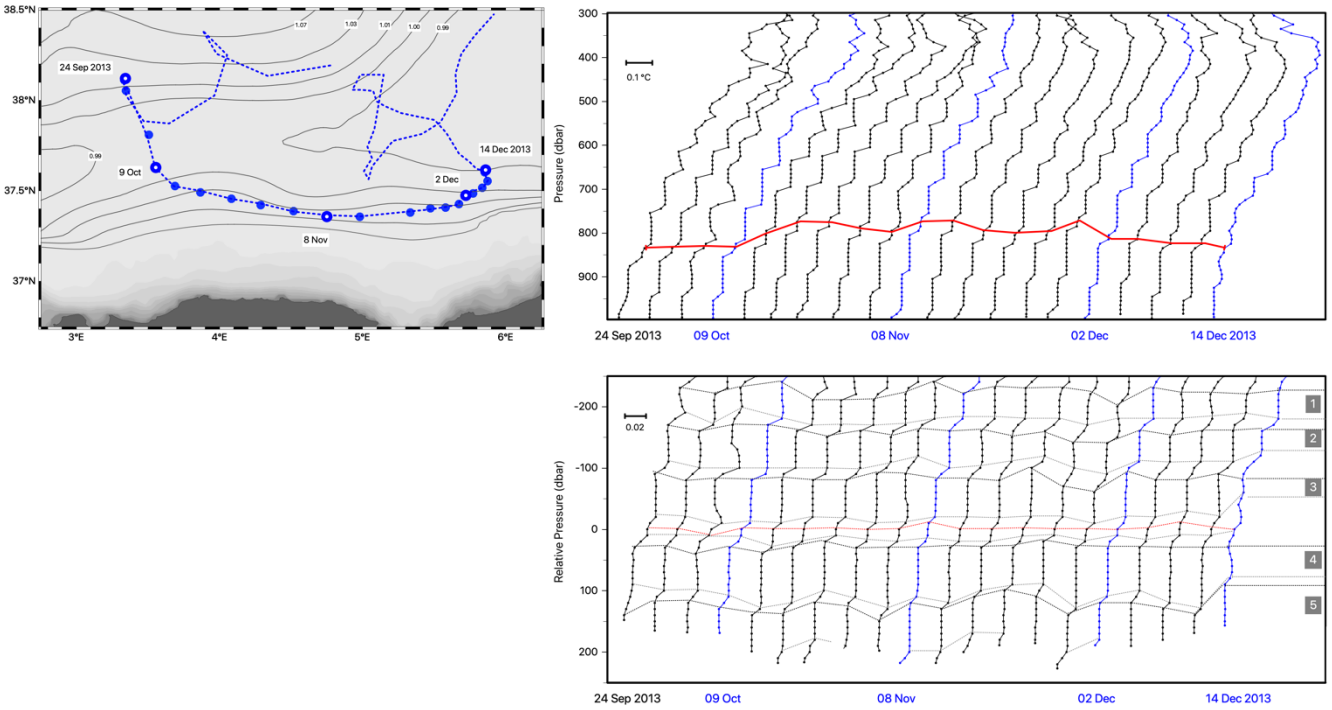

Figure 10: Successive CTD profiles collected by the float 6901513 between 24 September 2013 and 14 December 2013, with a vertical resolution of 10 dbar. The temperature profiles are shifted by 0.1°C (upper right panel), the salinity profiles are shifted by 0.02 (lower right panel). In x-axis, dates of the blue profiles, in correspondence with their location along the float trajectory (empty dots, left panel). In y-axis, pressure referenced to surface (upper right panel), or relative pressure referenced to the depth of the interface 3/4 indicated in red lines (lower right panel).

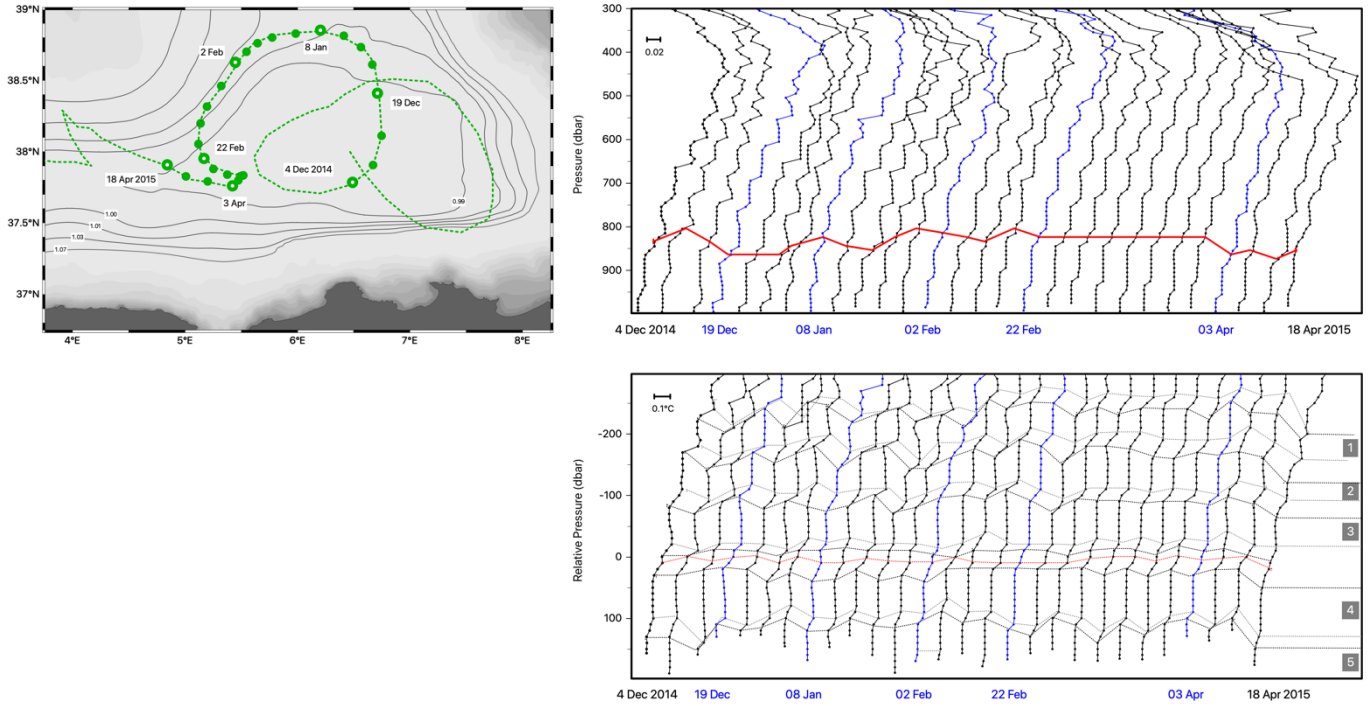

Figure 11: Successive CTD profiles collected by the float 6901600 between 4 December 2014 and 18 April 2015, with a vertical resolution of 10 dbar. The temperature profiles are shifted by 0.1°C (lower right panel), the salinity profiles are shifted by 0.02 (upper right panel). In x-axis, dates of the blue profiles, in correspondence with their location along the float trajectory (empty dots, left panel). In y-axis, pressure referenced to surface (upper right panel), or relative pressure referenced to the depth of the interface 3/4 indicated in red lines (lower right panel).

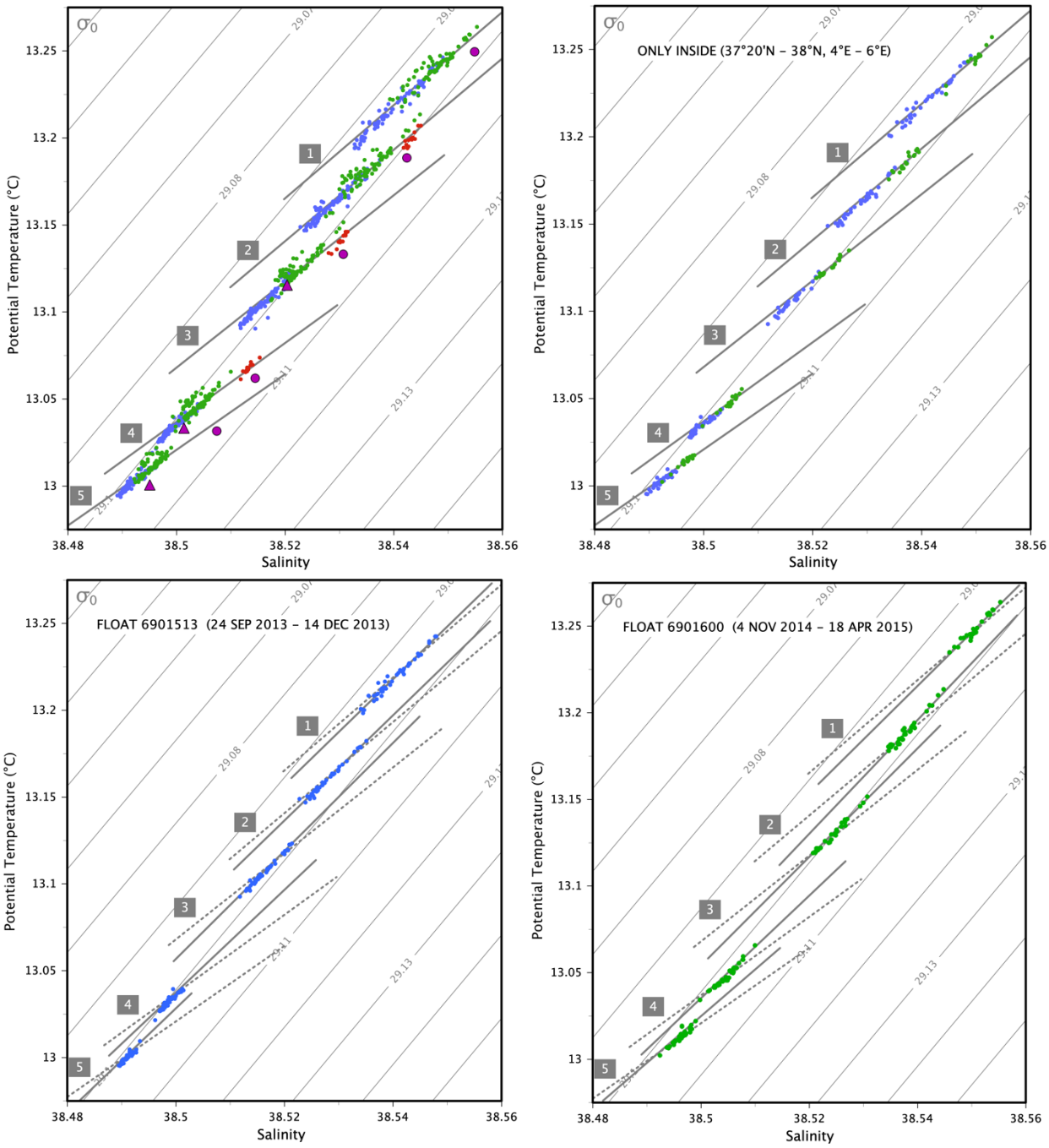

Figure 12: Temperature – salinity diagram of the layer properties. Floats in blue (6901513), green (6901600) and red (6902732); stations PEACETIME (2017) in purple dot, station SOMBA-GE (2014) in purple triangle. The layer numbering is the one of Table 4. The least square fit per layer is indicated in grey lines. Whole dataset (upper left panel), selection inside the box (37°20'N-38°N, 4°E-6°E) (upper right panel), and the two episodes in the lower panels. The least square fit of the upper left panel is reported in the lower panels with dotted lines.

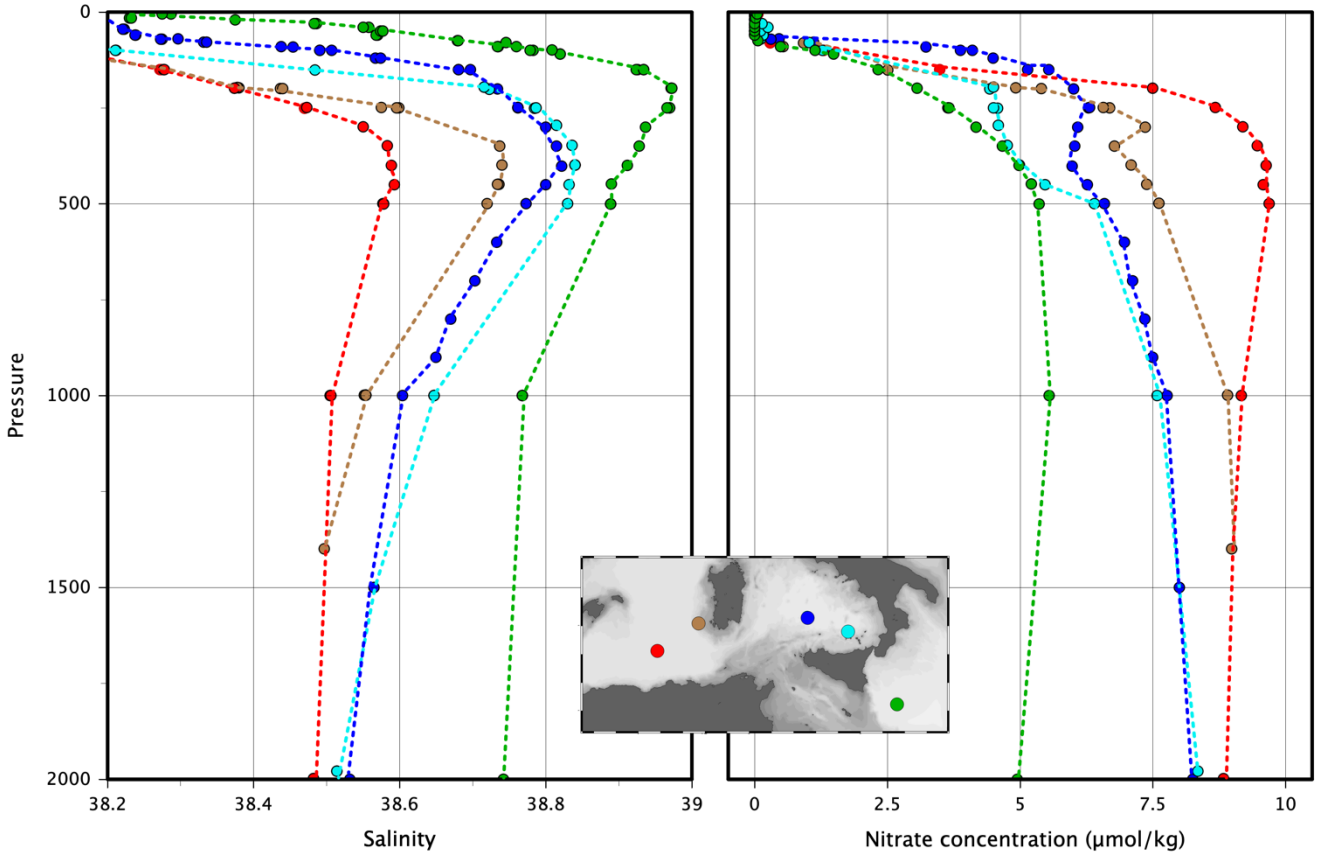

Figure 13: discrete profiles of salinity and nitrate (in µmol/kg) measured at bottle levels during the cruise PEACETIME. The station in the central Tyrrhenian Sea (dark blue dots) corresponds to the cast A reported in Figure 3. The station in the Algerian Basin (red dots) corresponds to the cast H reported in Figure 7.

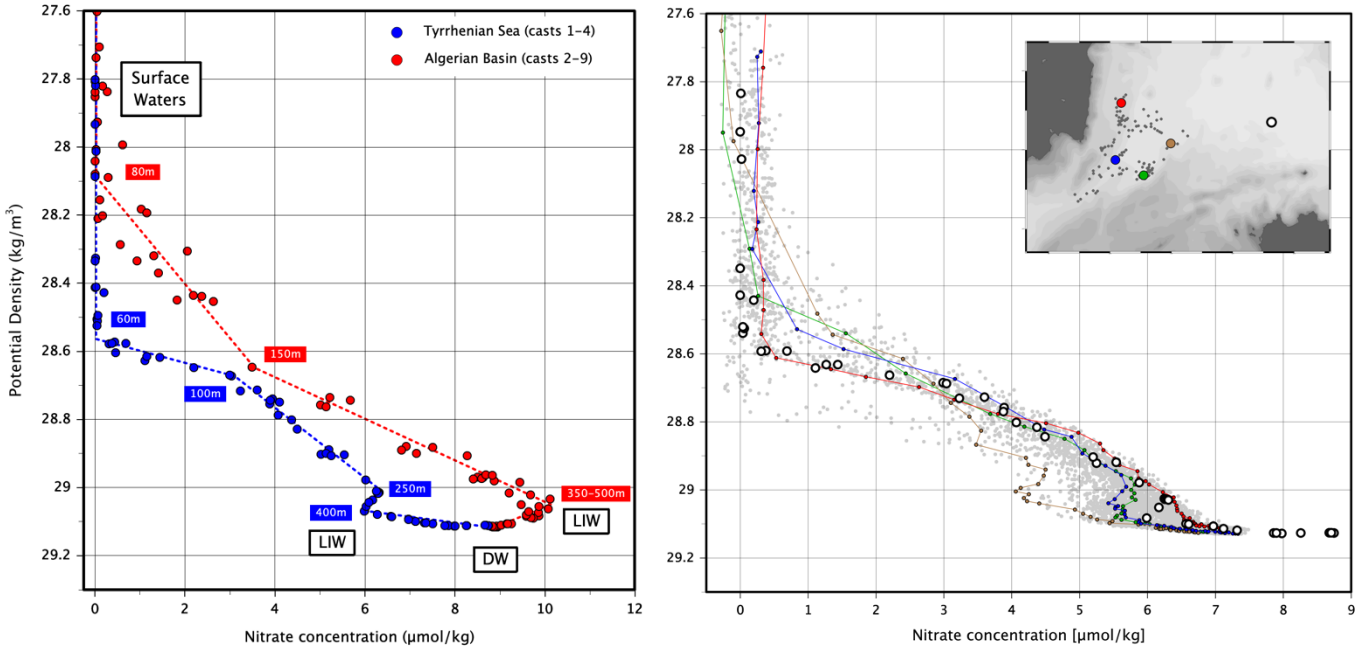

Figure 14: nitrate concentrations (in µmol/kg) against potential density. Left panel: Data at bottle levels collected during the cruise PEACETIME Blue dots: casts A-D in the Tyrrhenian Sea (locations indicated in Figure 3). Red dots: casts B-I in the Algerian Basin (locations indicated in Figure 7). Right panel: the cruise data (empty dots) and the float 6901769 data (grey dots). Float profiles of 3 October 2015 (red), 29 November 2016 (green), 27 December 2016 (brown), and 11 April 2017 (blue).

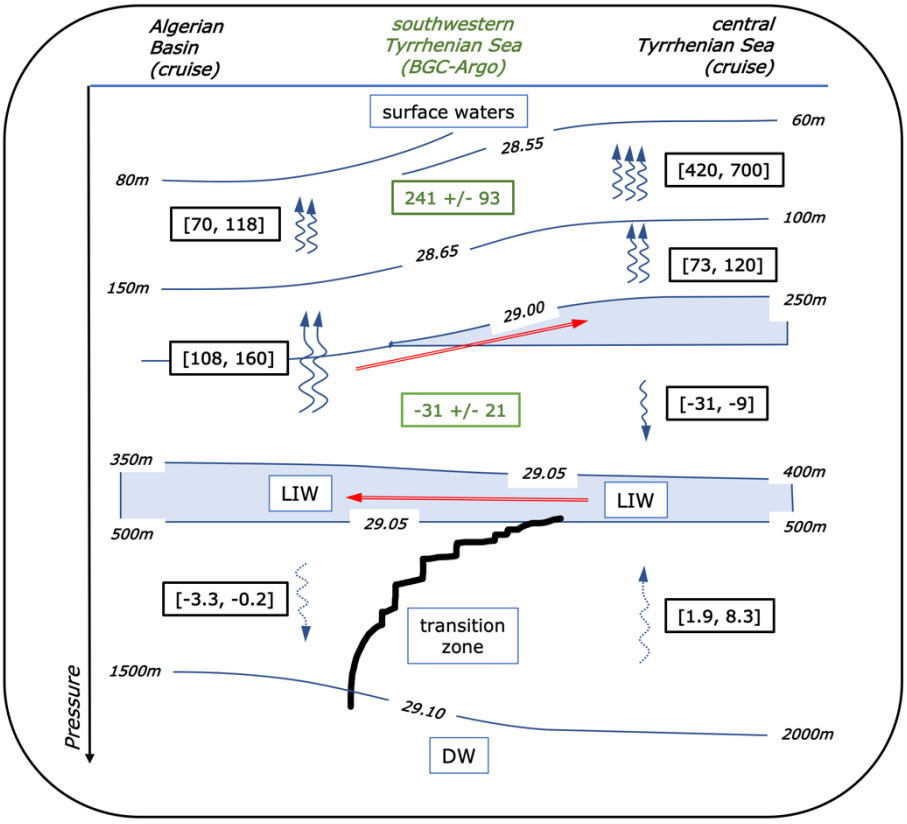

Figure 15: Vertical fluxes of nitrate F_{NO3} (in µmol/m^2/d) in presence of thermohaline staircases. Range of estimations reported from the Table 6 for the stations collected during PEACETIME (in black), or computed from the float 6901769 data (in green), with positive diffusive flux oriented upwards. Proposed isopycnal advection indicated in red arrows.